

# Open charm tomography of cold nuclear matter

I. Vitev,<sup>\*</sup> T. Goldman,<sup>†</sup> and M. B. Johnson<sup>‡</sup>

*Los Alamos National Laboratory, Theoretical Division and Physics Division, Los Alamos, NM 87545, USA*

J. W. Qiu<sup>§</sup>

*Department of Physics and Astronomy, Iowa State University, Ames, IA 50011, USA*

We study the relative contribution of partonic sub-processes to  $D$  meson production and  $D$  meson-triggered inclusive di-hadrons to lowest order in perturbative QCD. While gluon fusion dominates the creation of large angle  $D\bar{D}$  pairs, charm on light parton scattering determines the yield of single inclusive  $D$  mesons. The distinctly different non-perturbative fragmentation of  $c$  quarks into  $D$  mesons versus the fragmentation of quarks and gluons into light hadrons results in a strong transverse momentum dependence of anticharm content of the away-side charm-triggered jet. In p+A reactions, we calculate and resum the coherent nuclear-enhanced power corrections from the final-state partonic scattering in the medium. We find that single and double inclusive open charm production can be suppressed as much as the yield of neutral pions from dynamical high-twist shadowing. Effects of energy loss in p+A collisions are also investigated phenomenologically and may lead to significantly weaker transverse momentum dependence of the nuclear attenuation.

PACS numbers: 12.38.Cy; 12.39.St; 13.85.Ni; 24.85.+p

## I. INTRODUCTION

A useful probe of the dense nuclear matter created in collisions of heavy nuclei at the relativistic heavy ion collider (RHIC) is one that is sensitive to dynamical scales and can be both cleanly measured experimentally and reliably calculated theoretically. Because of color confinement, only hard probes, i.e. those with large momentum transfers, can be reliably calculated in the perturbation theory of Quantum Chromodynamics (QCD) [1, 2]. Experimental measurements of inclusive particle suppression [3, 4] are now able to test jet quenching theory out to transverse momenta of  $p_T \sim 20$  GeV [5]. On the other hand, typical dynamical scales of the nuclear matter produced in relativistic heavy ion collisions are on the order of hundreds of MeV, which is both much smaller than the scale of a hard probe and non-perturbative. Therefore, an ideal probe should be not only “hard” but also sensitive to this “soft” physics. Open charm production has a potential to satisfy these criteria because of the two distinctive scales of the open charm meson: the charm quark mass,  $m_c \sim 1.5$  GeV, a relatively hard scale, and the binding energy,  $\sim M_D - m_c \sim$  hundreds MeV, which may be relevant to the fragmentation and dissociation of  $D$  mesons.

Little quantitative understanding of medium effects exists for heavy-flavor production, due largely to the fact that the relevant data is quite sparse at present [6, 7] and inferred from the modified cross sections for non-photonic electrons. The experimental situation is rapidly

changing, however. In addition to introducing new mass scales, the advantages of using heavy quarks as probes also arise from the fact that once formed, heavy mesons live much longer ( $\sim 10^{-11}$  sec) than the duration of the QGP ( $\sim 10^{-23}$  sec), travel macroscopic distances away from the creation point and can be measured directly. Such precision measurements are not only facilitated by the boost at forward rapidities at RHIC and the LHC but also impacted by the non-negligible cold nuclear matter effects in this kinematic region [8, 9, 10, 11].

With this in mind, we extend the study of Refs. [10, 12, 13] to hadronic collisions with heavy-quark final states and consider single- and double-inclusive open charm production. Because of the quantitative importance of multiple scattering effects for inferring properties of the nuclear matter, the models of in-medium interactions should be subjected to experimental verification for heavy-flavor production. One may begin to gain confidence by applying the theoretical description of such effects to heavy ion collisions in simpler situations, such as proton-nucleus (p+A) scattering. In this case, plasma properties are not an issue and the main medium effect is, therefore, due to the multiple interactions in cold nuclei. The medium effects that we plan to investigate are also present in nucleus-nucleus (A+A) reactions during the interaction time  $\tau_{int.} = 2R_A/\gamma \ll \tau_{eq.} \ll \tau_{QGP}$  and cannot be neglected. Here  $R_A$  is the nuclear radius,  $\gamma$  is the Lorentz gamma factor of the nucleus,  $\tau_{eq.}$  is the equilibration time and  $\tau_{QGP}$  is the lifetime of the plasma.

Multiple scattering affects the nuclear cross sections in various ways depending on how parton propagation is modified by the medium as the partons enter into, and emerge from the hard scattering. At one extreme, when the scattering from the medium is largely incoherent, the parton modification is dominated by transverse momentum broadening [8]. At the other extreme, when the longitudinal momentum transfer is small com-

<sup>\*</sup>Electronic address: ivitev@lanl.gov

<sup>†</sup>Electronic address: tgoldman@lanl.gov

<sup>‡</sup>Electronic address: mbjohnson@lanl.gov

<sup>§</sup>Electronic address: jwq@iastate.edu

pared to the length of the path of the parton as it propagates through the nucleus, the scattering becomes coherent which can lead to attenuation, or shadowing. The coherent limit is described differently in different approaches [14, 15, 16]. In our work its effects are calculated in terms of nuclear-enhanced power corrections [10, 12, 13]. We have shown that these could account for a large portion or all of nuclear shadowing observed at small Bjorken  $x_B$  in lepton-nucleus deep inelastic scattering (DIS). They also contribute to the sizable suppression of forward rapidity single- and double-inclusive hadron production at RHIC [17, 18]. As the heavy quark introduces a new mass scale, the dependence of the nuclear-size-enhanced power corrections on this scale needs to be elucidated.

Inelastic interactions of partons propagating in nuclear matter lead to energy loss in both the incoherent [19] and the coherent [20, 21] regimes. While jet quenching effects are best established in A+A reactions [3, 4, 5], it was recently shown that energy loss can lead to hadron suppression in d+Au collisions at forward rapidities at RHIC [22]. In a preliminary study [23] we approximated the effects of such energy loss by a rapidity shift. We will demonstrate that partonic implementation of energy loss, suggested in [8], gives qualitatively similar results but also allows extraction of the fraction of the energy lost by an average parton in cold nuclear matter. Finally, we point out that the multi-parton dynamics discussed in this work will become even more important in p+A, and consequently A+A, collisions at the LHC.

Our paper is organized as follows: In Section II we outline the theoretical framework for the calculation of observables in hadronic collisions in which elastic, inelastic and coherent multiple scattering effects in hot and cold nuclear matter can be naturally incorporated. In Section III we calculate to lowest order (LO) the contribution of the various partonic sub-processes to single inclusive  $D$  meson production and  $D$  meson-triggered inclusive di-hadron yields in “elementary” nucleon-nucleon interactions. The light hadron/charm meson fraction in the away-side charm-triggered jet is shown to be sensitive to the transverse momentum of the associated particle. The effect of nuclear-enhanced power corrections and their physical interpretation is discussed in Section IV. The suppression of both  $D$  meson production cross sections and of  $D$  meson-triggered correlations at forward rapidity at RHIC are also calculated. We discuss in Section V the effects of energy loss in cold nuclear matter and demonstrate that the resulting nuclear suppression has a different transverse momentum behavior when compared to dynamical high-twist shadowing. Our conclusions are given in Section VI. In Appendix A we explicitly calculate the LO parton scattering cross sections that contribute to single and double inclusive charm production. Appendix B contains the details of the factorization of the quark and gluon coherent scattering from the non-perturbative high-twist matrix elements. We also demonstrate how to reduce these high-twist matrix elements to the scale

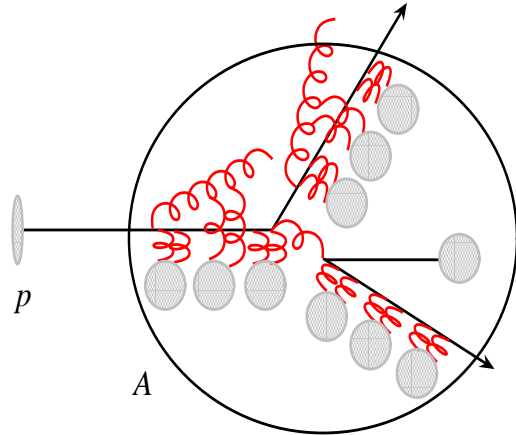


FIG. 1: Schematic representation of the initial- and final-state elastic, inelastic and coherent multiple parton scattering that give the nuclear  $A^{n/3}$ -enhanced corrections similar to Eq. (2) for proton-nucleus collisions in the nuclear rest frame.

of power corrections per individual nucleon enhanced by the nuclear size.

## II. THEORETICAL FRAMEWORK

The interpretation of the plethora of results from past, present and future heavy ion experiments necessitates a reliable theoretical framework for the calculation of a variety of moderate and large transverse momentum observables,  $p_T^2 \gg \Lambda_{\text{QCD}}^2$ , that can be systematically extended to incorporate corrections arising from the many body nuclear dynamics. The perturbative QCD factorization approach [1] provides such a tool and expresses the observable hadronic cross sections as

$$\sigma_{\text{hadronic}} = \sigma_{\text{partonic}}(x_i, z_j; \mu_r; \mu_{fi}, \mu_{dj}) \otimes \left\{ \prod_i \phi_{i/h_i}(x_i, \mu_{fi}) \right\} \otimes \left\{ \prod_j D_{h_j/j}(z_j, \mu_{dj}) \right\}, \quad (1)$$

where  $\otimes$  denotes the standard convolution over the internal kinematic variables in the reaction. In Eq. (1)  $\mu_r$ ,  $\mu_{fi}$  and  $\mu_{dj}$  are the renormalization, factorization and fragmentation scales, respectively.  $\phi_{i/h_i}(x_i, \mu_{fi})$  is the distribution function (PDF) of parton “ $i$ ” in the hadron  $h_i$  and  $D_{h_j/j}(z_j, \mu_{dj})$  is the fragmentation or decay function (FF) of parton “ $j$ ” into hadron  $h_j$ . Factorization not only separates the short- and long-distance QCD dynamics but implies universality of the PDFs and FFs and infrared safety of the hard scattering partonic cross sections.

In the nuclear environment, corrections in the basic perturbative formulas arise from the possible nuclear de-

Type of scattering	Transverse momentum dependence of the nuclear effect
<i>Elastic (incoherent)</i>	Inclusive 1-particle production: Cronin effect, enhancement at moderate $p_T$ , disappears at high $p_T$ Inclusive 2-particle production: di-jet acoplanarity, broadening of away-side correlations
<i>Inelastic (final-state)</i>	Inclusive 1-particle production: suppression at all $p_T$ , weak $p_T$ dependence, amplified near the kinematic bounds Inclusive 2-particle production: suppression of high $p_T$ correlations, enhancement of low $p_T$ correlations
<i>Inelastic (initial-state)</i>	Inclusive 1-particle production: suppression at all $p_T$ , weak $p_T$ dependence, amplified near the kinematic bounds Inclusive 2-particle production: same as inclusive 1 particle production
<i>Coherent (t-channel)</i> <i>(u-channel)</i>	Inclusive 1-particle production: suppression at low $p_T$ , disappears at high $p_T$ , pronounced $p_T$ dependence Inclusive 2-particle production: same as inclusive 1 particle production
<i>Coherent (s-channel)</i>	Inclusive 1-particle production: enhancement at low $p_T$ , disappears at high $p_T$ , pronounced $p_T$ dependence Inclusive 2-particle production: same as inclusive 1 particle production

TABLE I: Effect of elastic, inelastic and coherent multiple scattering on the transverse momentum dependence of single and double inclusive hadron production in the perturbative regime.

pendence of PDFs and FFs as well as multiple soft parton scattering. These corrections may be enhanced by the nuclear size and the density of the quark-gluon plasma (QGP) in the deconfined phase. In DIS, cold nuclear matter effects can be systematically organized in the framework of the factorization approach as follows:

$$\begin{aligned}
\sigma_{\text{hadron}} = & \\
& \sigma_0^{(2)} \left( 1 + C_1^{(2)} \alpha_s + C_2^{(2)} \alpha_s^2 + C_3^{(2)} \alpha_s^3 + \dots \right) T^{(2)} \\
& + \frac{\sigma_0^{(4)}}{Q^2} \left( 1 + C_1^{(4)} \alpha_s + C_2^{(4)} \alpha_s^2 + C_3^{(4)} \alpha_s^3 + \dots \right) T^{(4)} \\
& + \frac{\sigma_0^{(6)}}{Q^4} \left( 1 + C_1^{(6)} \alpha_s + C_2^{(6)} \alpha_s^2 + C_3^{(6)} \alpha_s^3 + \dots \right) T^{(6)} \\
& + \dots
\end{aligned} \tag{2}$$

In Eq. (2)  $T^{(i)}$  are the twist “i” non-perturbative matrix elements.  $Q^2$  is a typical virtuality, for example in hadron collisions we find  $Q^2 = -\hat{t}$ ,  $-\hat{u}$  or  $-\hat{s}$ . Standard higher order calculations at leading twist, such as NLO, NNLO correspond to the determination of the coefficient functions  $C_i^{(2)}$  in Eq. (2). Soft in-medium interactions are controlled by new scales, such as the transverse momentum transfer squared per mean free path  $\mu^2/\lambda$  [5, 8] and the scale of higher twist per nucleon  $\xi^2$  [12, 13]. While we can write a formal expansion in  $\alpha_s$  for these quantities, it is usually subject to theoretical uncertainties and slow

convergence of the perturbation series. For the purpose of this paper we consider the new scales to be properties of the medium and keep track only of the nuclear size  $A^{1/3}$ , or  $L$ , enhancement. In DIS, high-twist shadowing corresponds to the identification and resummation of the nuclear-size-enhanced higher-twist terms,  $\sigma_0^{(i)} T^{(i)}$  in Eq. (2). We emphasize that in p+A collisions, illustrated in Fig. 1, neither initial- nor final-state interactions can be neglected since the coupling strength to the medium is qualitatively the same.

From a phenomenological point of view, it is useful to classify the multiple parton interactions based on their experimentally observable effect on the hadronic spectra and the correlated yield of leading di-hadrons from away-side jets, or di-hadron correlations. Table II provides guidance, consistent with our current knowledge and results from this work, to the correspondence between the nuclear modification to the cross sections measured in A+B collisions and the binary scaled p+p result,

$$R_{AB}^{(n)} = \frac{d\sigma_{AB}^{h_1 \dots h_n} / dy_1 \dots dy_n dp_{T_1} \dots dp_{T_n}}{\langle N_{AB}^{\text{coll}} \rangle d\sigma_{NN}^{h_1 \dots h_n} / dy_1 \dots dy_n dp_{T_1} \dots dp_{T_n}}. \tag{3}$$

In Eq. (3)  $\langle N_{AB}^{\text{coll}} \rangle$  can be evaluated from an optical Glauber model.

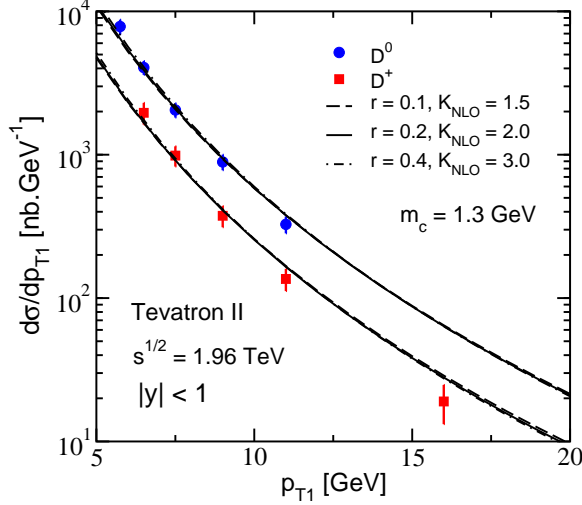


FIG. 2: Cross section for  $D^0$  and  $D^+$  charm meson production to LO in perturbative QCD at  $\sqrt{s} = 1.96$  TeV. Three approximately equivalent pairs of a phenomenological  $K$ -factor and the  $D$  meson fragmentation parameter  $r$  are shown.

### III. $D$ MESON PRODUCTION AND CORRELATIONS IN LOWEST ORDER PQCD

Nuclear-enhanced power corrections to the hadronic cross sections are sensitive to the partonic structure of the underlying hard scattering event. We first evaluate the differential cross sections for open charm production and open-charm-triggered di-hadron correlations in the Born approximation. Calculations to match the fixed order (FO) perturbative results to resummed logarithms of the type  $\alpha_s^n (a_k \ln p_T/m_c)^k$  up to next-to-leading log (NLL),  $n = 2$ , exist that treat flavor as “heavy” [24], based on the assumption  $\phi_{c/N}(x, \mu_f) \equiv 0$ . We include the charm contribution from the nucleon wave-function explicitly since this approach leads to a faster convergence of the perturbation series [25]. Our goal is to investigate the fractional contribution of partonic sub-processes to the differential open charm cross section with power corrections in mind. We naturally limit our discussion to transverse momenta larger than the heavy quark mass  $p_{T1}, p_{T2} \geq m_c$ .

#### A. Partonic sub-processes for inclusive $D$ meson production and $D$ meson-triggered correlations

The kinematics that underlies hadronic collisions is introduced by the following example of LO jet production in the collinear factorization approach:

$$\frac{d\sigma_{NN}^{j_1(c)j_2(d)}}{dy_c dy_d d^2 p_{Tc} d^2 p_{Td}} = K_{NLO} \sum_{ab} \frac{\delta(\Delta\varphi - \pi) \delta(p_{Tc} - p_{Td})}{p_{Td}} \times \frac{\phi_{a/N}(x_a) \phi_{b/N}(x_b)}{x_a x_b} \frac{\alpha_s^2}{S^2} |\overline{M}_{ab \rightarrow cd}|^2. \quad (4)$$

In Eq. (4)  $S = (p_A + p_B)^2$  is the squared center of mass energy of the hadronic collision,  $x_a = p_a^+/p_A^+$ ,  $x_b = p_b^-/p_B^-$  are the lightcone momentum fractions of the incoming partons and  $\phi_{a/N}(x_a)$ ,  $\phi_{b/N}(x_b)$  are the distribution function of partons  $a, b$  in the nucleon. In this work we use the CTEQ6.1 LO PDFs [26]. In the double collinear approximation the jets are produced back-to-back at LO in  $\alpha_s$ . The running of the strong coupling constant  $\alpha_s$  is also taken to lowest order.

The power corrections to single- and double-inclusive hadron production are manifest only at small and moderate momentum transfers [10, 12], where the effect of the heavy quark mass may not be negligible. PDFs, based on global QCD analysis, use massless evolution kernels to derive the  $Q^2$  dependence of the heavy,  $c$  and  $b$ , quark distributions [26]. Systematic corrections of the type  $m_q^2/Q^2$  have so far proven difficult to implement. To reconcile the use of parton distributions for charm quarks with  $m_q = 0$  with a final state where  $m_q \neq 0$  we calculate the relevant matrix elements in Appendix A.

With  $m_{Ti} = \sqrt{p_{Ti}^2 + m_i^2}$ ,  $i = c, d$  we identify the lightcone momentum fractions:

$$x_a = \frac{1}{\sqrt{S}} (m_{Tc} e^{y_c} + m_{Td} e^{y_d}), \quad (5)$$

$$x_b = \frac{1}{\sqrt{S}} (m_{Tc} e^{-y_c} + m_{Td} e^{-y_d}). \quad (6)$$

From Eq. (4), after fragmentation into charm mesons, and integration over the away-side jets, we obtain the single inclusive  $D^0$ ,  $D^+$  meson production cross section:

$$\frac{d\sigma_{NN}^{D_1}}{dy_1 d^2 p_{T1}} = K_{NLO} \sum_{abcd} \int_{\mathcal{D}} dy_2 \int_{\mathcal{D}} dz_1 \times \frac{1}{z_1^2} D_{D_1/c}(z_1) \frac{\phi_{a/N}(x_a) \phi_{b/N}(x_b)}{x_a x_b} \frac{\alpha_s^2}{S^2} |\overline{M}_{ab \rightarrow cd}|^2. \quad (7)$$

Here

$$\mathcal{D} = \{(x_1 \in [0, 1]) \cap (x_2 \in [0, 1]) \cap (z_1 \in [0, 1])\};$$

$z_1 = p_{T1}/p_{Tc}$  and we have chosen the factorization, and renormalization scales  $\mu_f = \mu_r = \sqrt{p_{Tc}^2 + m_c^2}$ . Only charm quark fragmentation into  $D^0$ ,  $D^+$  mesons is considered.

In this paper we take  $D_{D/c}(z_1)$  for vector and pseudo-scalar mesons from [27]. The shape of the heavy quark fragmentation function is determined by the value of the non-perturbative parameter  $r$ . Smaller values of  $r$  correspond to harder fragmentation. The decay of the vector states  $D^{0*}$ ,  $D^{+*}$  into  $D^0$ ,  $D^+$  with the experimentally measured branching ratios is taken into account. To study the relation between the phenomenological  $K$ -factor in Eq. (7) and the non-perturbative parameter  $r$  [27] in  $D$  meson fragmentation we compare the calculated  $D^0$  and  $D^+$  cross sections to the Tevatron Run II  $\sqrt{s} = 1.96$  TeV data [28] in Fig. 2. We find that three different combinations ( $K_{NLO} = 1.5$ ,  $r = 0.1$ ), ( $K_{NLO} = 2$ ,

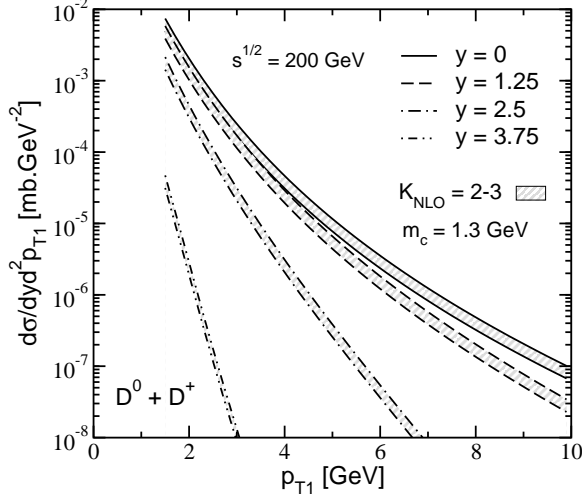


FIG. 3: The cross section for  $D^0 + D^+$  charm meson production to LO in perturbative QCD at  $\sqrt{s} = 200$  GeV in  $p + p$  collisions at RHIC with  $K_{NLO} = 2 - 3$  and  $r = 0.2$ . The differential cross section is shown in four rapidity bins:  $y = 0, 1.25, 2.5$  and  $3.75$ .

$r = 0.2$ ) and ( $K_{NLO} = 3, r = 0.4$ ) yield little difference in the single inclusive charm meson spectrum. We note that for the same choice of the parameter  $r = 0.1$ , a LO calculation with standard  $\phi_{c/N}(x, \mu_f) \neq 0$  gives open charm cross sections similar to the ones from a NLO calculation that treats flavor as “heavy”. In this paper we adhere to the more conservative choice  $r = 0.2$ . Taking into account an estimated  $\sim 50\%$  uncertainty of the  $K$ -factors at the smaller  $\sqrt{s} = 200$  GeV, we show the differential  $D^0 + D^+$  cross sections in  $p + p$  in Fig. 3 for several rapidity bins:  $y = 0, 1.25, 2.5$  and  $3.75$ . These are the baseline differential distributions relative to which the effects of power corrections and energy loss can be studied. The uncertainty of the choice at RHIC ( $K_{NLO} = 2.5, r = 0.2$ ) cancels in the nuclear modification ratios, Eq. (3).

In hadronic collisions, heavy quark pair production proceeds via the “flavor creation” sub-processes, gluon-gluon fusion,  $gg \rightarrow c\bar{c}$ , and light quark-antiquark annihilation,  $q\bar{q} \rightarrow c\bar{c}$ , at lowest order in the strong coupling constant  $\alpha_s$ . Since the gluon density is much larger than the quark and antiquark distributions at a small parton momentum fraction,  $x$ , the gluon fusion sub-process is believed to dominate charm production in hadronic collisions at collider energies. However, for inclusive single charm production, a single charm (or anticharm) quark can be created via the “flavor excitation” sub-processes,  $cg \rightarrow cg$  and  $cq \rightarrow cq$ . Although the charm parton distribution is small,  $\phi_{c/N}(x) \ll \phi_{g/N}(x)$ , such processes can be amplified by the matrix elements  $|\overline{M}_{ab \rightarrow cd}|^2$ . In Eq. (7), over most of the available phase space

$$\left| \frac{\hat{u}}{\hat{t}} \right| \approx \left| \frac{\hat{s}}{\hat{t}} \right| = L_1 \gg 1, \quad \text{or} \quad \left| \frac{\hat{t}}{\hat{u}} \right| \approx \left| \frac{\hat{s}}{\hat{u}} \right| = L_2 \gg 1, \quad (8)$$

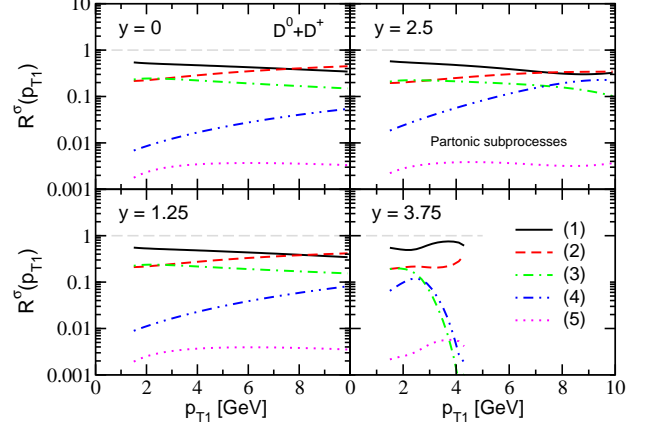


FIG. 4: Fractional contribution of partonic sub-processes (i) to moderate and high  $p_{T1}$   $D^0 + D^+$  meson production in  $\sqrt{s} = 200$  GeV  $p + p$  collisions at rapidities  $y = 0, 1.25, 2.5$  and  $3.75$ . We considered (1)  $cg \rightarrow cg$  (solid line), (2)  $cq(\bar{q}) \rightarrow cq(\bar{q})$  (dashed line), (3)  $gg \rightarrow c\bar{c}$  (dot-dashed line), (4)  $q\bar{q} \rightarrow c\bar{c}$  (double dot-dashed line) and (5)  $c\bar{c} \rightarrow c\bar{c}$  (dotted line). Note the dominance (except at the highest values of  $p_{T1}$ ) of the  $cg \rightarrow cg$  channel.

where  $L_1, L_2$  are numerically large. From the analysis in Appendix A, we find that the leading power behavior in  $L_1$  of hard parton scattering for the first case in Eq. (8) is

$$\langle |\mathcal{M}_{gg \rightarrow c\bar{c}}|^2 \rangle \sim \frac{1}{6} L_1 \quad \text{versus} \quad (9)$$

$$\langle |\mathcal{M}_{cg \rightarrow cg}|^2 \rangle \sim \frac{8}{9} L_1^2, \quad \langle |\mathcal{M}_{cq \rightarrow cq}|^2 \rangle \sim 2 L_1^2. \quad (10)$$

Clearly, there is large,  $\propto L_1$ , amplification of the scattering rate in Eq. (10) relative to Eq. (9).

The fractional weight of the partonic sub-processes to open charm production can be fully studied through the ratio:

$$R^\sigma(p_{T1}) = \frac{d\sigma_{ab \rightarrow cd}^{D_1}}{dy_1 d^2 p_{T1}} \bigg/ \frac{d\sigma_{tot}^{D_1}}{dy_1 d^2 p_{T1}}. \quad (11)$$

Numerical results for the single inclusive charm cross sections, Eq. (7), are shown in Fig. 4 at  $\sqrt{s} = 200$  GeV. We find that the dominant  $D$  meson production mechanism is the scattering of the heavy quark from the wavefunction of the nucleon (or nucleus) on gluons,  $cg \rightarrow cg$ . Heavy on light quark scattering,  $cq(\bar{q}) \rightarrow cq(\bar{q})$ , also contributes significantly to the cross section. In these processes the charm anti-quarks from the nucleon wavefunction end up in the fragmentation region near the beam rapidity. While gluon fusion,  $gg \rightarrow c\bar{c}$ , is non-negligible it is also not the main channel for single inclusive open charm production. We have checked that  $R^\sigma(p_{T1})$  is practically independent of the interplay between  $K_{NLO}$  and the hardness  $r$  of the  $c$  quark fragmentation into  $D$  mesons.

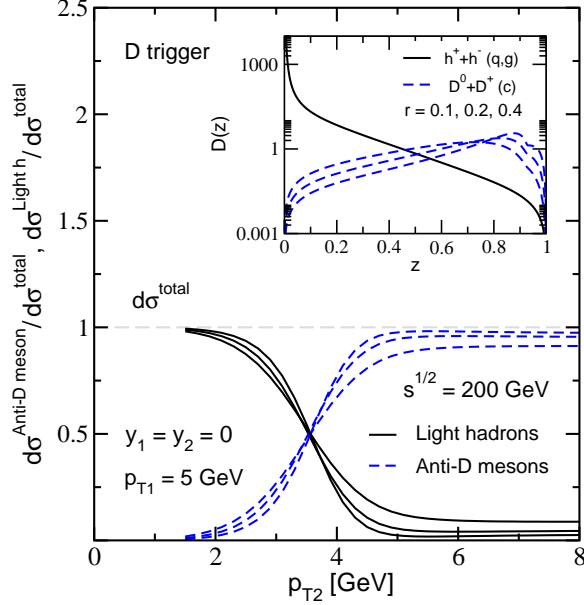


FIG. 5: Contribution of light hadrons and anticharm mesons to the fractional production cross section for  $p_{T1} = 5$  GeV  $D^0 + D^+$  meson-triggered away-side correlations for  $y_1 = y_2 = 0$ . The insert illustrates the difference in the fragmentation of light quarks and gluons into hadrons versus that for the  $c$  quark into charm mesons. Three different values for the non-perturbative fragmentation parameter  $r = 0.1, 0.2$  and  $0.4$  were used.

### B. Hadron composition of $D$ meson-triggered away-side jets

We now proceed to charm meson-triggered di-hadron correlations in away-side jets, which have not been studied previously. For pairs of hadrons with large opening angle between them,  $\Delta\varphi = \varphi_1 - \varphi_2 \sim \pi$ , including charm-anticharm and charm-hadron correlations, we find [10, 29]:

$$\frac{d\sigma_{NN}^{D_1 h_2}}{dy_1 dy_2 dp_{T1} dp_{T2}} = K_{NLO} \sum_{abcd} 2\pi \int_D \frac{dz_1}{z_1} D_{D_1/c}(z_1) D_{h_2/d}(z_2) \times \frac{\phi_{a/N}(x_a) \phi_{b/N}(x_b)}{x_a x_b} \frac{\alpha_s^2}{S^2} |\overline{M}_{ab \rightarrow cd}|^2, \quad (12)$$

where

$$D = \{(x_1 \in [0, 1]) \cap (x_2 \in [0, 1]) \cap (z_1 \in [0, 1] \cap (z_2 \in [0, 1]))\}.$$

The fragmentation scale for light hadrons in Eq. (12) is set to  $\mu = p_{Td}/z_2$  and  $z_2 = z_1 p_{T2}/p_{T1}$ . We use FFs from [30] for  $\pi^\pm, K^\pm$  and  $p(\bar{p})$ . In the calculations that follow, we also include charm quark fragmentation into light hadrons. For the charm anti-quark,  $D_{\bar{D}/\bar{c}}(z) = D_{D/c}(z)$ .

The expectation for non-trivial  $p_{T2}$  dependence of charm-triggered away-side correlations is based on

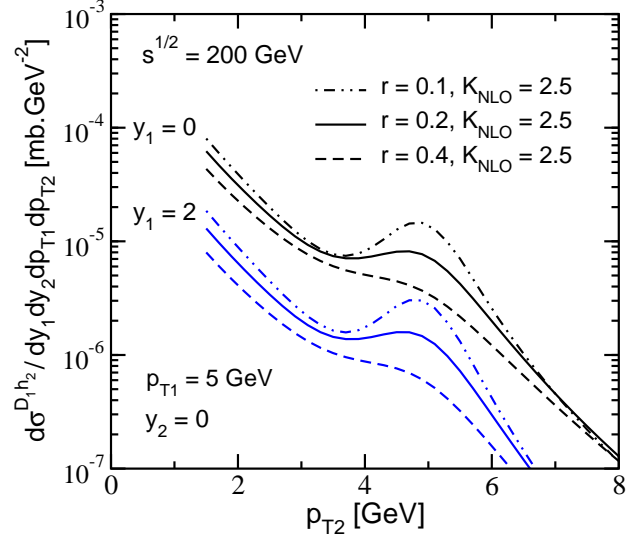


FIG. 6: The double inclusive hadron production cross section at RHIC for a  $D^0 + D^+$  trigger at  $p_{T1} = 5$  GeV. Three different combinations of  $r$  and  $K_{NLO}$  are studied. Two different rapidity gaps  $y_1 - y_2 = 0, 2$  are shown for comparison. The characteristic “hump” represents hard  $\bar{c}$  fragmentation into  $\bar{D}$  mesons.

the very different behavior with respect to  $z = p^{hadron}/p^{parton}$  of the fragmentation functions of partons into light hadrons [30] compared to those of heavy quarks into charm and beauty mesons [27]. The insert in Fig. 5 shows that while light hadrons favor soft decays of their parent partons, heavy quark fragmentation is very hard. For  $z \sim 0.6 - 0.9$  there is more than an order of magnitude enhancement in the decay probabilities  $D_{D^0/c}(z) + D_{D^+/c}(z)$  relative to  $(1/N) \sum_{i=1,N} (D_{\pi^\pm/i} + D_{K^\pm/i} + D_{p(\bar{p})/i})$ , where  $i$  runs over the light and charm quarks, antiquarks and the gluon.

Triggering on a  $D$  meson fixes the momentum of the charm quark much more reliably than does triggering on a light hadron [10, 29] in studying away-side correlations. The non-perturbative fragmentation therefore controls the yields of di-hadrons versus the associated momentum  $p_{T2}$  and the abundances of the different particle species. Fig. 5 shows our prediction for the hadronic composition of the  $D^0 + D^+$ -triggered away-side jet. At transverse momenta significantly smaller than the trigger transverse momentum,  $p_{T2} \ll p_{T1}$ , the away-side jet is dominated by pions, kaons and protons. At transverse momenta  $p_{T1} \simeq p_{T2}$ , the away-side jet is expected to be dominated almost completely by  $\bar{D}^0$  and  $D^-$  mesons. Since there is little sensitivity to the choice of  $r$ , our prediction is robust and can be used as a test of the production mechanism of heavy quarks.

Fig. 6 shows the behavior of the  $D$ -meson-triggered di-hadron cross section, Eq. (12). The differential spectrum cannot be described by a single power law for  $p_{T2} \simeq p_{T1}$ . In the case of hard fragmentation, for ex-



ample  $r = 0.1$ , the double inclusive distribution can even be non-monotonic as a function of the associated particle momentum  $p_{T_2}$ . The characteristic “hump” is associated with the  $\bar{c}$  fragmentation into  $\bar{D}^0$  and  $D^-$ . This signature is unique for heavy quark triggers and is seen to be independent of rapidity. For pion or unidentified hadron triggers one expects a smooth power law behavior as a function of  $p_{T_2}$  [10, 29]. We conclude, through the comparison of Figs. 2 and 6, that charm-triggered correlations provide a much more powerful handle on the hardness of  $D_{D/c}(z)$  than does the single inclusive spectrum.

In summary, even in p+p collisions at RHIC and the LHC, triggering on charm or beauty mesons can provide constraints on the heavy quark production and fragmentation mechanisms that are not accessible via the Tevatron single inclusive data. Such measurements may already be possible at RHIC using electron or muon triggers as proxies for heavy quarks [31, 32].

#### IV. NUCLEAR-ENHANCED POWER CORRECTIONS TO OPEN CHARM PRODUCTION

In this section we focus on the effects of coherence that arise from the multiple soft scattering of the partons that participate in the hard interaction. The processes where such effects can be cleanly studied are deeply inelastic scattering (DIS), illustrated in Fig. 7(a), and Drell-Yan. If the longitudinal momentum transfer along a fixed direction becomes small, the probe will interact simultaneously with more than one nucleon, due to the uncertainty principle. In a frame where the longitudinal size of the exchanged virtual meson is given by  $l_c = 1/xP$  the Lorentz contracted nucleon has longitudinal size  $2r_0/\gamma = 2r_0/(P/m_N)$ . The critical value of the momentum fraction for the onset of coherence can be easily estimated to be  $x_N = 1/(2r_0m_N) \sim 0.1$  [12, 13]. For  $x \leq 0.01$ , the interaction with all of the nucleons at the same impact parameter  $b$  is coherent, given the small transverse size  $A_\perp = 1/Q^2$ ,  $Q^2 \geq m_N^2$ , determined by the virtual probe. The multiple final-state interactions with these nucleons are mediated via the field of soft gluons and are formally suppressed by a power of the squared momentum transfer  $1/Q^2$  for each additional coherent scattering. The resummed contributions form all powers in  $1/Q^2$  have the effect of a dynamical generation of a quark or gluon mass as we shall see below.

In the case of hadronic collisions there is indeed a similarity with the DIS dynamics in the final-state rescattering of the struck, small  $x_b$  parton from the nucleus, as shown in Fig. 7(b). Such nuclear-enhanced power corrections lead to suppression of the single and double inclusive hadron production cross sections at forward rapidity as long as the coherence criterion is satisfied [10].

#### A. Physical interpretation

The physical interpretation of the resummed nuclear-enhanced power corrections is most transparent in the example of neutrino-nucleus scattering because of the presence of a physical mass scale  $M$  in the *final* state in some of the sub-processes [13]. Even in the absence of final-state interactions, the charged current  $s$ -quark to  $c$ -quark transition,  $s \pm W^\pm \rightarrow c$ , requires rescaling of the value of Bjorken  $x_B = Q^2/2m_N\nu$  in the parton distribution functions

$$x = x_B \rightarrow x = x_B \left(1 + \frac{M^2}{Q^2}\right). \quad (13)$$

Since  $x$  represents the lightcone momentum fraction carried by the struck quark, Eq. (13) expresses the conversion of the larger initial parton energy into the constituent mass of the heavy quark. In Ref. [13], using Dirac equations of motion, we showed that the physical mass and the dynamical power corrections commute and therefore the two effects add. The corresponding change in the value of Bjorken  $x$  is

$$\begin{aligned} x = x_B \rightarrow x = x_B & \left(1 + \frac{\xi^2(A^{1/3} - 1)}{Q^2} + \frac{M^2}{Q^2}\right) \\ &= x_B \left(1 + \frac{m_{dyn}^2}{Q^2} + \frac{M^2}{Q^2}\right) \\ &= x_B \left(1 + \frac{M^2}{Q^2}\right) \left(1 + \frac{m_{dyn}^2}{M^2 + Q^2}\right). \end{aligned} \quad (14)$$

Our resummed higher-twist corrections rescale the momentum fraction,  $x_B$ , in Eq. (14) in a manner identical to the modification arising from the constituent heavy quark mass, Eq. (13). We identify  $m_{dyn}^2 = \xi^2(A^{1/3} - 1)$  with the dynamical mass [10, 12, 13] generated by propagation of the struck parton through the nuclear background chromo-magnetic field. We remark that this effect, which we calculated in QCD, is analogous to the generation of dynamical mass for electrons propagating in a strong electro-magnetic field [34]. For  $x_B < 0.1$ ,

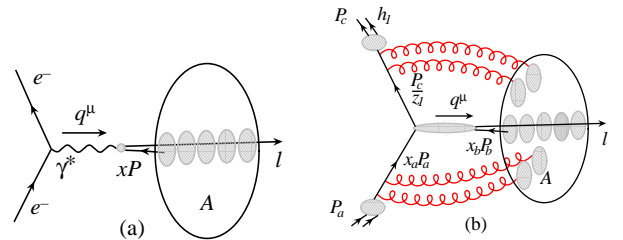


FIG. 7: Coherent multiple scattering of the struck parton in deeply inelastic scattering (a) and in proton-nucleus collisions (b). Notice the difference between  $p + A$  and DIS in terms of the multiple initial- and final-state scattering of the incoming and outgoing partons (“a” and “c”).

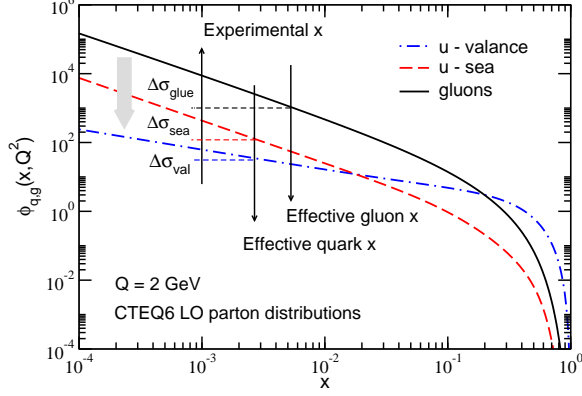


FIG. 8: Effects of rescaling of the momentum fraction  $x$  illustrated on the example of the lowest order CTEQ6 parton distribution functions for valence and sea  $u$ -quarks. Gluons rescatter in the final-state to lowest order only in hadronic collisions and are included for completeness. The effective parton distributions or partonic flux are reduced after the rescaling of the momentum fraction. We used  $Q^2 = 4 \text{ GeV}^2$  and the large rescaling in  $x$  is for purposes of illustration only.

due to coherence,  $m_{dyn}^2$  has to be incorporated in the underlying kinematics of the hard scattering, Eq. (14). For values of  $x_B > 0.1$  rescattering of the struck parton still occurs but the vector meson exchange is localized to one nucleon. The elastic final-state interactions vanish by unitarity upon integrating over the full phase space for the hadronic fragments,  $X$ .

The mechanism behind the reduction of the deeply inelastic inclusive scattering cross section and the differential hadron production cross sections is illustrated schematically in Fig. 8. PDFs are falling functions of the momentum fraction  $x$ :

$$\begin{aligned} \phi_v(x) &\propto x^{-1/2+\delta_v}, & \text{valence quarks,} \\ \phi_s(x) &\propto x^{-1+\delta_s}, & \text{sea quarks,} \\ \phi_g(x) &\propto x^{-1+\delta_g}, & \text{gluons,} \end{aligned} \quad (15)$$

where  $|\delta_{v,s,g}| \ll 1$ . The evaluation of the parton distribution function at an effectively larger value of  $x$  leads to a reduction of the cross section,  $-\Delta\sigma$  [12, 13]. From Eq. (15) it follows that the same dynamically generated parton mass for quarks apparently produces a different reduction in the sea and valence contributions to the DIS cross sections,  $-\Delta\sigma_{\text{sea}} \simeq -2\Delta\sigma_{\text{valence}}$ . If a gluon scatters coherently in the final state, the generated dynamical mass is  $C_A/C_F = 9/4$  larger than the dynamical mass for a quark due to the larger average squared color charge. Consequently, the observable “shadowing” of gluons is substantially larger than that for sea quarks, despite the very similar low- $x$  behavior of the PDFs in Eq. (15),  $-\Delta\sigma_{\text{gluon}} \simeq -9/4\Delta\sigma_{\text{sea}}$ . We can, therefore,

derive a hierarchy of dynamical high-twist shadowing,

$$S(x, Q^2) = \left| \frac{-\Delta\sigma(x, Q^2)}{\sigma(x, Q^2)} \right|$$

$$S_v(x, Q^2) < S_s(x, Q^2) < S_g(x, Q^2), \quad (16)$$

for cross sections with multiple scattering dominated by valence quarks, sea quarks or gluons, respectively.

## B. Power corrections in $p+A$ reactions with heavy quark final states

A detailed derivation of nuclear-enhanced power corrections in proton(deuteron)-nucleus collisions is given in Appendix B. In this subsection we summarize the main results. Unlike structure functions in DIS, hadronic collisions involve a more complicated momentum flow even in LO tree level diagrams. This requires isolating the  $x_b$  dependence of the integrand in Eqs. (7) and (12) in the function

$$F_{ab \rightarrow cd}(x_b) = \frac{\phi_{b/N}(x_b) |M_{ab \rightarrow cd}|^2}{x_b}. \quad (17)$$

Since we use the standard on-shell hard scattering matrix elements  $|M_{ab \rightarrow cd}|^2$  reproduced in Appendix A we obtain an upper limit on the dynamical high-twist shadowing. The scale of high-twist corrections on an *individual* nucleon  $\xi^2 = 0.09 - 0.12 \text{ GeV}^2$  is fixed by the world’s data on deep inelastic scattering on a wide range of nuclear targets [12], including the shadowing in the structure functions,  $F_2$ , and the enhancement in the longitudinal structure function,  $F_L$ , relative to the result at leading twist. This is the same scale that was used to predict the  $Q^2$ -dependent suppression of the small  $x$  structure functions in neutrino scattering on iron (Fe) targets measured by the NuTeV collaboration [35]. Since  $\xi^2$  is constrained from final-state quark scattering, we account for the representation of parton  $d$  in hadronic reactions by the color factor  $C_d$  on a process-by-process basis. The values are  $C_{q(\bar{q})} = 1$  and  $C_g = C_A/C_F = 9/4$  for a quark (antiquark) and a gluon, respectively.

The forward rapidity particle production in  $p(d)+A$  collisions is analogous to DIS, and resumming the coherent scattering with multiple nucleons is equivalent to a shift of the momentum fraction of the active parton from the nucleus which leads to a net suppression of the cross sections. The hard scattering scale is given here by  $\hat{t} = q^2 = (x_a p_A - p_c/z_1)^2$ , and for Eqs. (7) and (12) we derive the following nuclear modification:

$$F_{ab \rightarrow cd}(x_b) \Rightarrow F_{ab \rightarrow cd} \left( x_b \left[ 1 + C_d \frac{\xi^2 (A^{1/3} - 1)}{-\hat{t} + m_d^2} \right] \right). \quad (18)$$

We denote by  $A$  the atomic mass number of the nucleus even though it is labeled as hadron “ $B$ ” or “ $b$ ”. The



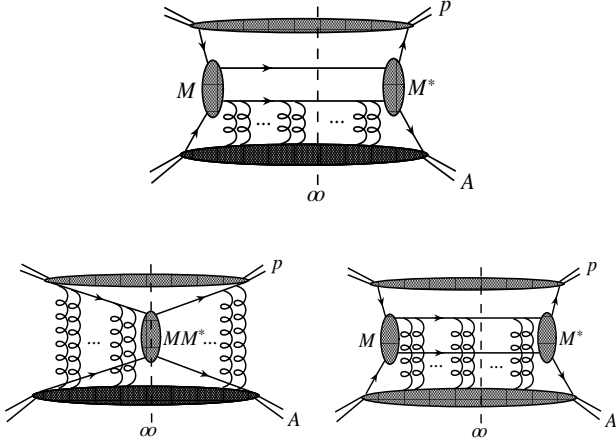


FIG. 9: Multiple coherent scattering of the incoming and outgoing partons in p+A reactions in the  $t$ -,  $s$ - and  $u$ -channels, respectively.

$\hat{t}$ -dependence of this shift in Eq. (18) indicates that the attenuation increases in the forward rapidity region but disappears at large transverse momenta. We note that the effect of the mass of the final-state parton, for example a charm quark, in Eq. (18) is precisely the same as in the DIS case [13], Eq. (14).

While we have focused in detail on the power corrections in the  $t$ -channel, it should be noted that the coherent initial- and final-state interactions of the incoming parton from the proton, see the bottom diagrams in Fig. (9), can also be calculated. The results that we present here are analogous to Eq. (18),

$$F_{ab \rightarrow cd}(x_b) \Rightarrow F_{ab \rightarrow cd} \left( x_b \left[ 1 + C_a \frac{\xi^2 (A^{1/3} - 1)}{-\hat{s}} \right] \right), \quad (19)$$

$$F_{ab \rightarrow cd}(x_b) \Rightarrow F_{ab \rightarrow cd} \left( x_b \left[ 1 + C_c \frac{\xi^2 (A^{1/3} - 1)}{-\hat{u} + m_c^2} \right] \right). \quad (20)$$

In Eqs. (19) and (20)  $C_a$  and  $C_c$  are the numerical coefficients analogous to  $C_d$  corresponding to partons  $a$  and  $c$ , respectively. By direct comparison of the nuclear- $A^{1/3}$ -enhanced power corrections in Eqs. (18), (19) and (20) it is easy to see that in the forward rapidity region  $|\hat{t}| \ll |\hat{s}|, |\hat{u}|$  only DIS-like dynamical shadowing corrections are important.

On the other hand, in processes with no strong final-state interactions, such as the Drell-Yan, coherent multiple initial-state scattering can give only *enhancement* of the cross section, as shown in Eq. (19), because of the rescaling of  $x_b$  to smaller versus larger values. Such result is also easily understandable since an incoming parton with large dynamically generated mass prior to the hard scatter has to carry a smaller fraction of the nucleon momentum in order to produce particles in the final state

with fixed momentum. Thus, initial-state multiple soft interactions without energy loss always lead to a Cronin effect [8] independently of whether they are treated as coherent or not.

The derivations given here are critical to elucidating the dynamical origin of nuclear effects in high energy hadronic reactions. We have shown through explicit calculation that such effects are process dependent and may change their sign. Therefore, these are *not* factorizable as a part of the PDFs and FFs.

The cross section for single and double inclusive hadron production can be calculated from Eqs. (7) and (12) via the substitutions Eqs. (18), (19) and (20) in minimum bias reactions. We recall that the  $A^{1/3}$ -enhanced scale of higher twist,  $\xi^2 = 0.12 \text{ GeV}^2$ , has the minimum bias geometry included. For specific centrality classes we account for the varying nuclear thickness along the line of parton propagation as follows:

$$A^{1/3} \rightarrow A^{1/3} \frac{T_A(b)}{T_A(b_{\text{min.bias}})}, \quad (21)$$

where  $T_A(b) = \int_{-\infty}^{\infty} \rho_A(z, b) dz$ .

### C. Numerical results

To illustrate the similarities and differences between massless and massive final-state partons, we carry out a comparative study of the effect of power corrections on single and double inclusive  $\pi^0$  and  $D$  meson production. The left panels of Fig. 10 show the suppression of the low and moderate  $p_{T_1}$  neutral pion cross section relative to the binary scaled p+p result, Eq. (3), from high-twist shadowing. The nuclear modification factor is shown for two different forward rapidities,  $y_1 = 1.25, 2.5$ , in  $\sqrt{s} = 200 \text{ GeV}$  d+Au collisions at RHIC. At transverse momenta  $p_{T_1} = 1.5 \text{ GeV}$  the suppression can be as large as 25% but disappears toward higher  $p_{T_1}$  due to the power law nature of the effect.  $R_{dAu}(p_{T_1})$  also shows non-zero rapidity dependence with the effect increasing at forward rapidities. For comparison, we show the PHENIX measurement of the nuclear modification of muons coming from the decay of charged hadrons in mid-central d+Au reactions at  $y_1 = 1.8$  is shown [17]. Coherent power corrections cannot fully account for the nuclear suppression measured by experiment. The discrepancy becomes larger at higher transverse momenta. The bottom left panel of Fig. 10 shows the centrality dependence of coherent power corrections for light pions. From Eq. (21), we see that in central collisions the larger nuclear thickness generates correspondingly larger dynamical parton mass leading to larger suppression of the cross sections.

The right panels of Fig. 10 show the calculated suppression of  $D^0 + D^+$  mesons (and equivalently,  $\bar{D}^0 + D^-$  mesons), in deuteron-gold collisions at RHIC. It should be noted that the nuclear modification is very similar

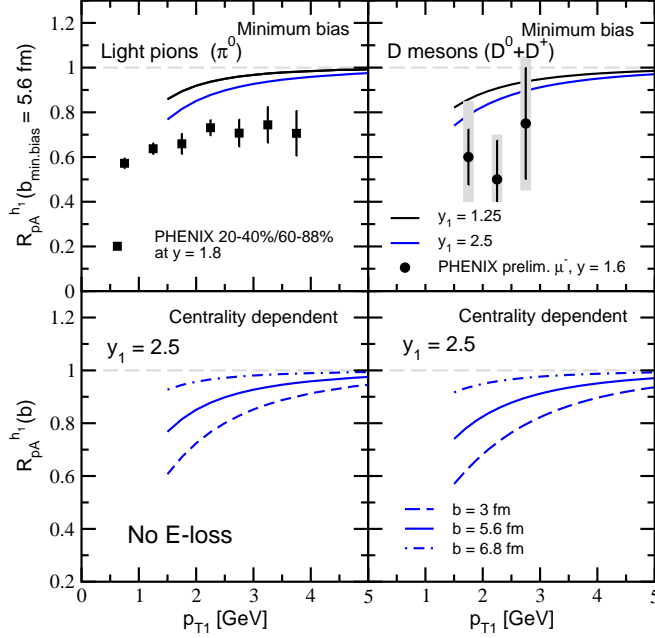


FIG. 10: Top: suppression of the single inclusive hadron production rates in d+Au reactions versus  $p_T$  for rapidities  $y_1 = 1.25$  (smaller attenuation) and  $y_1 = 2.5$  (larger attenuation). Bottom: impact parameter dependence of the calculated nuclear modification for central,  $b = 3$  fm, minimum bias,  $b_{\text{min.bias}} = 5.6$  fm and peripheral,  $b = 6.8$  fm, collisions. The scale of higher twist per nucleon  $\xi^2 = 0.12$  GeV<sup>2</sup>. Data is from PHENIX [17, 36]. Theory does not include energy loss.

to or slightly larger than that for  $\pi^0$ . The reason for this similarity is that in both cases the dominant channel of hadron production is via quarks scattering on gluons, which have the same (large) color singlet coupling to the medium,  $C_d = 9/4$  in Eq. (18). In addition, the typical momentum fraction,  $z_1$ , which enters in the determination of the hard scale,  $\hat{t} \propto 1/z_1$ , is slightly larger for the  $D$  mesons. Preliminary PHENIX data on the modification of  $\mu^-$ 's coming from the decay of heavy flavor at  $y = 1.6$  in cold nuclear matter is provided as a reference [36]. Although the error bars are large,  $D$  mesons seem to be suppressed as much as light hadrons. This attenuation effect is larger than predicted by power corrections alone.

Our results for the dynamical shadowing effects in inclusive two-particle measurements at large angle  $\Delta\phi \sim \pi$  are given in Fig. 11. We have chosen  $p_{T_1} = p_{T_2}$  and the same rapidity of the trigger hadron,  $y_1$ , as in Fig. 10. The associated hadron was chosen at rapidity  $y_2 = 0$  to facilitate the study of di-jets with a large rapidity gap. The left panels of Fig. 11 show that  $\pi^0 - \pi^0$  modification in the nuclear medium follows qualitatively the suppression of single inclusive pions as shown in Fig. 10. The right panels of Fig. 11 illustrate the effects of coherent power corrections on  $(D^0 + D^+) - (\bar{D}^0 + D^-)$  pair production. In this case we have a heavy  $\bar{c}$  quark scattering coherently in the final state. At  $p_{T_1} = p_{T_2} = 1.5$  GeV  $\sim m_c$ ,

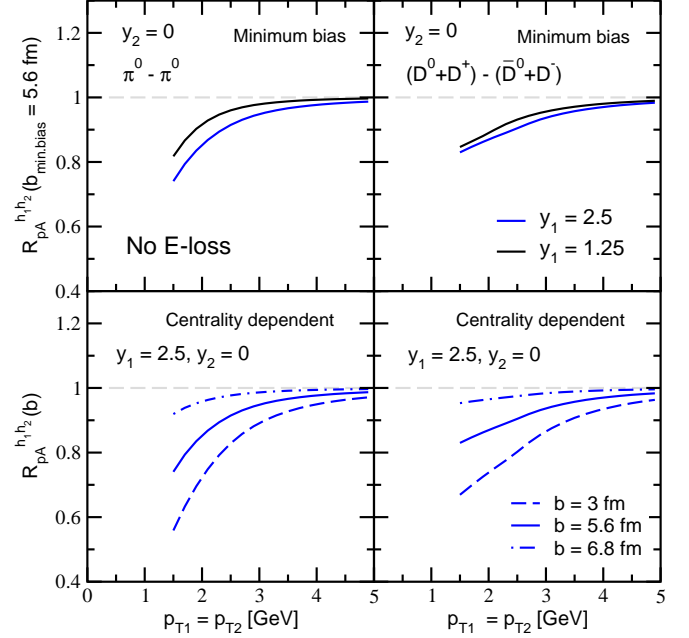


FIG. 11: Top: suppression of double inclusive hadron production rates in d+Au reactions versus  $p_T$  for trigger and associated hadrons of the same transverse momentum but different rapidities:  $y_1 = 1.25$  (smaller attenuation) and  $y_1 = 2.5$  (larger attenuation) for the trigger and  $y_2 = 0$  for the associated hadron. Bottom: impact parameter dependence of the calculated nuclear modification for central,  $b = 3$  fm, minimum bias,  $b_{\text{min.bias}} = 5.6$  fm and peripheral,  $b = 6.8$  fm, collisions. The scale of higher twist per nucleon  $\xi^2 = 0.12$  GeV<sup>2</sup>. Theory does not include energy loss.

the effect of the heavy quark mass on the power corrections that we derived in Appendix B is noticeable, see Eq. (18). At higher transverse momenta the mass effect is not relevant. Naively, we would expect that  $\bar{D}D$  pair production would be less suppressed due to the quark versus the gluon color singlet coupling to the medium,  $C_d = 1$  versus  $9/4$ . However, in light hadron pair production the momentum fractions  $z_1, z_2$  are significantly smaller [38] than in single inclusive measurements and  $D$  meson production. Therefore the relevant hard scale,  $\hat{t}$ , in  $\bar{D}D$  pair production is smaller which amplifies the effect of the dynamical heavy quark mass.

## D. Discussion

The nuclear-size-enhanced power corrections that enter this work are the result of a tree-level QCD calculation and represent the effect of multiple coherent scatterings of the outgoing partons with the gluon field of the nucleus. The strength of this interaction is specified by a universal parameter,  $\xi^2$ , which is related to the limiting soft gluon distribution of a nucleon in the nucleus. Once  $\xi^2$  is specified, the effect of coherent scattering for

all partons, heavy and light quarks as well as gluons, is completely determined. In particular, when the coherence length, defined as the inverse of the longitudinal momentum transfer, becomes comparable to the nuclear size, these power corrections acting on partons in the final state suppress the hadron cross sections.

In Ref. [16], the effects of coherence are determined by multiple scattering, and this approach is therefore, in principle, quite similar to ours. The following points of difference should, however, be noted. Using a Green-function description of quark-gluon Fock states in combination with the Glauber-Gribov formulation of nuclear shadowing, it is shown there how multiple diffractive scattering of gluons suppresses the gluon distribution in a nucleus when the coherence length in gluon-dominated processes begins to exceed the inter-particle spacing, thus providing an estimate of gluon shadowing. The scale of the suppression is fixed by, among other things, the triple-pomeron coupling  $G_{3P} = 3 \text{ mb/GeV}^2$ . The small triple pomeron coupling suggests a rather confined gluon cloud of valence quarks, and this weakens gluon shadowing and delays its onset. This gluon shadowing is also "leading twist", i.e., weakly dependent on  $Q^2$ , vanishing logarithmically as  $Q^2 \rightarrow \infty$ .

## V. ENERGY LOSS IN COLD NUCLEAR MATTER

In Fig. 1 and the discussion in the previous section we clarified that, in the presence of a nucleus, final-state rescattering of the struck small  $x$  parton with its remnants exhausts the similarity between hadronic collisions, such as p+A and A+A, and DIS [10]. In  $\ell + A$  (DIS), the multiple interactions of the incoming leptons are suppressed by powers of  $\alpha_{em}/\alpha_s$  relative to the struck parton scattering. In contrast, in p+A and A+A the initial- and final-state scattering of the incoming quarks and gluons are equally strong. Nuclear modification, in particular jet energy loss associated with the suppression of particle production, cannot be neglected. In a model of Sudakov suppression, Ref. [22], it was shown that the effect is amplified at forward Feynman  $x$ ,  $x_F \rightarrow 1$ .

### A. Evidence for energy loss in cold nuclear matter

To illustrate the importance of energy loss, we study the nuclear modification of hadron production over a large range of center of mass energies and momentum fractions  $x_b$ . In one extreme, at  $\sqrt{s} = 200 \text{ GeV}$  d+Au collisions at RHIC, the STAR collaboration observed a factor of 3 suppression of  $\pi^0$  production relative to the binary collision scaled p+p result [18]. Figure 12 shows that dynamical high-twist shadowing, constrained by the DIS data down to values of Bjorken  $x_B \sim 10^{-4}$ , underpredicts the nuclear attenuation by a factor of 2.

Next, we implement the presently known incoherent

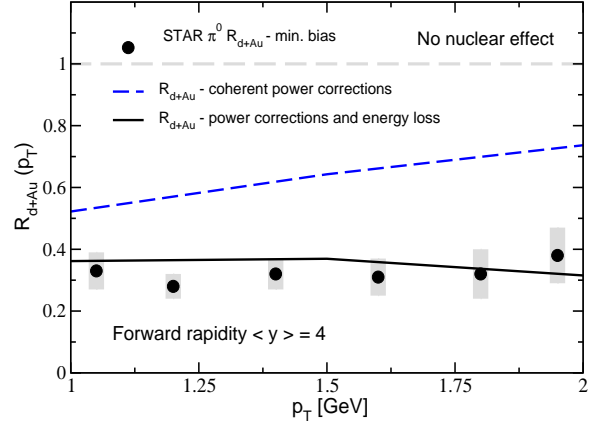


FIG. 12: Suppression of  $\pi^0$  production at  $y = 4$  for d+Au collisions at  $\sqrt{s_{NN}} = 200 \text{ GeV}$  at RHIC [18]. Calculations of dynamical shadowing with and without cold nuclear matter energy loss are shown.

limit of energy loss for on-shell partons first derived in [19]. The double differential gluon intensity spectrum per scattering reads:

$$\frac{\omega dN_g^{(1)}}{d\omega d^2\mathbf{k}} \propto \frac{\alpha_s}{\pi^2} \frac{\mathbf{q}_1^2}{\mathbf{k}^2(\mathbf{k} - \mathbf{q}_1)^2}, \quad (22)$$

where  $\mathbf{k}$  is the transverse momentum of the radiative gluon,  $\mathbf{q}_1$  is the transverse momentum transfer from the medium and  $\omega$  is the gluon energy. The two characteristics of this radiative energy loss that we use are  $\Delta E \propto E$  and  $\Delta E \propto L/\lambda$  in the case of multiple interactions. Jet quenching before the partonic hard scatter implies that in p+A and A+A reactions quarks and gluons carry larger fraction  $x_a$  of the nucleon momentum than in p+p collisions [8]:

$$\epsilon = \frac{\Delta E}{E} \propto \frac{L}{\lambda} = \kappa A^{1/3}, \quad (23)$$

$$\phi_{q,g/N}(x, \mu_f) \rightarrow \phi_{q,g/N}\left(\frac{x}{1-\epsilon}, \mu_f\right). \quad (24)$$

Fitting Eq. (23) to the data, we find  $\kappa = 0.0175$  for minimum bias reactions implying that an average parton loses  $\sim 10\%$  of its energy in a large nucleus such as Au or Pb. The variation of  $\kappa$  with centrality in the Bertsch-Gunion model is given by the nuclear thickness,  $T_A(b)$ , in a manner similar to the variation of the nuclear-enhanced power corrections. Figure 12 shows that such energy loss implementation gives good quantitative agreement with the forward rapidity suppression measured by STAR.

At the other extreme, the CERN NA35 fixed target experiment with  $y_{cm} = 3$  measured hadron production in d+Au reactions at  $\sqrt{s_{NN}} = 19.4 \text{ GeV}$  [33]. Although there is a factor  $\sim 100$  difference in the values of  $x_b$ , the STAR data were taken at much more forward  $y$  than the NA35 data, the same rapidity asymmetry is observed as at RHIC. We take  $R_y$ , the ratio of hadron spectra in

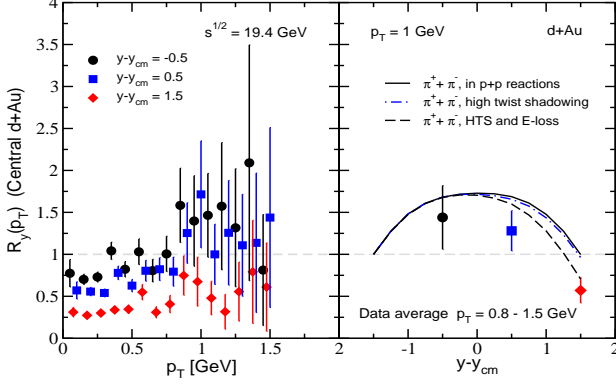


FIG. 13: Left panel: nuclear modification at three different rapidities  $y - y_{cm}$  in  $\sqrt{s_{NN}} = 19.4$  GeV d+Au collisions. Data is from NA35 [33]. Right panel: theoretical calculations of charged pion production in p+p and d+Au collisions with high-twist shadowing (HTS) and energy loss compared to the experiment.

different rapidity bins defined as

$$R_y(p_T) = \frac{d\sigma^h(y)}{dy d^2p_T} \bigg/ \frac{d\sigma^h(y_{base})}{dy d^2p_T}, \quad (25)$$

as a measure of cold nuclear matter effects. The left panel of Fig. 13 shows this forward rapidity suppression of negative hadrons relative to the baseline  $y - y_{cm} \approx -1.5$  production cross section. The right panel of Fig. 13 shows the deviation of the data in  $p_T = 0.8 - 1.5$  GeV interval from the symmetric p+p distribution around  $y_{cm}$ . Dynamical shadowing calculations [10] give  $< 5\%$  effect at this energy in this rapidity range. Leading-twist shadowing parameterizations are also not compatible with the asymmetry in the data [15]. Conversely, the implementation of energy loss in cold nuclear matter leads to much larger suppression at forward rapidity and significant improvement in the theoretical description of the data in Fig. 13. We conclude that such low energy p+A measurements [33] remove the ambiguity of what nuclear effects dominate the forward rapidity suppression in heavy ion collisions.

### B. Application of energy loss to D meson production in proton-nucleus collisions

Having investigated the largest dynamic range of measurements in proton(deuteron)-nucleus reactions accessible to perturbative QCD calculations, we return to  $D$  meson production and correlations at RHIC. We use the same fractional energy loss  $\epsilon = \Delta E/E$  as in Figs. 12 and 13. The forward rapidity boost  $E = m_T \cosh y_1 \gg m_c$  allows one to neglect the effect of the charm quark mass on  $\Delta E$ . Single inclusive  $\pi^0$  and  $D^0 + D^+$  suppression at rapidities  $y_1 = 1.25, 2.5$  and minimum bias, central and peripheral d+Au collisions at RHIC are shown in Fig. 14. In this case very good agreement between

the QCD theory incorporating cold nuclear matter effects and the PHENIX measurement of muons coming from the decay of light hadrons [17] is achieved. We find that the magnitude of the  $D$  meson suppression is similar to that of pions. It is also comparable with the first forward rapidity results on heavy quark nuclear modification in d+Au reactions at RHIC [36]. In Fig. 15 we also show the result of our calculations for the  $\pi^0 - \pi^0$  and  $(D^0 + D^+) - (\bar{D}^0 + D^-)$  mesons pair production at large angles. The same rapidity gaps,  $\Delta y = y_1 - y_2$ , and centralities as in Fig. 11 were used. Nuclear modification of inclusive two particle production is seen to follow closely that of single inclusive hadrons.

There are similarities between the calculations that only include resummed nuclear-enhanced power corrections, Figs. 10 and 11, and the calculations that do not neglect energy loss in cold nuclear matter, Figs. 14 and 15. Both effects are generated through multiple parton scattering in the medium and lead to suppression of the rate of hard scattering. In both cases single inclusive particle production and large angle di-hadron correlations are similarly attenuated. Like all nuclear many body effects these increase with the centrality of the collision. The difference in the resulting nuclear modification is that high-twist shadowing arises from the coherent final-state scattering of the struck small  $x_b$  parton of the nucleus and disappears as a function of the transverse momentum. The energy loss considered here arises from the initial-state inelastic scattering of the incoming large  $x_a$  parton from the proton(deuteron) and leads to a suppression which is much more  $p_T$  independent. By comparing our results for inclusive one- and inclusive two-particle production we see that

$$\frac{R_{d+A}^{(2)}(p_{T1} = p_{T2})}{R_{d+A}^{(1)}(p_{T1})} = \frac{\frac{d\sigma_{dAu}^{h_1 h_2}/dy_1 dy_2 dp_{T1} dp_{T2}}{\langle N_{dAu}^{coll} \rangle d\sigma_{NN}^{h_1 h_2}/dy_1 dy_2 dp_{T1} dp_{T2}}}{\frac{d\sigma_{dAu}^{h_1}/dy_1 dp_{T1}}{\langle N_{dAu}^{coll} \rangle d\sigma_{NN}^{h_1}/dy_1 dp_{T1}}} \approx 1. \quad (26)$$

Deviation from unity may arise due to specific choices of  $p_{T1}, p_{T2}$  and improved theoretical calculations of the parton color charge, system size and jet energy dependence of  $\Delta E$  in Eq. (23). Both calculations presented in this paper, are consistent with the lack of *significant* modification of the per trigger yield in d+Au reactions relative to p+p [37].

## VI. CONCLUSIONS

In this paper we have systematically studied inclusive  $D$  meson production and  $D$  meson-triggered di-hadron yields in p+p and p(d)+A reactions.

At collider energies, we have found that while  $D\bar{D}$  pair production is dominated by heavy quark flavor creation processes, such as gluon-gluon fusion  $gg \rightarrow c\bar{c}$  and light quark-antiquark annihilation  $q\bar{q} \rightarrow c\bar{c}$ , single inclusive  $D$  (and  $\bar{D}$ ) meson production is controlled by radiatively generated charm quarks in the nucleon wave

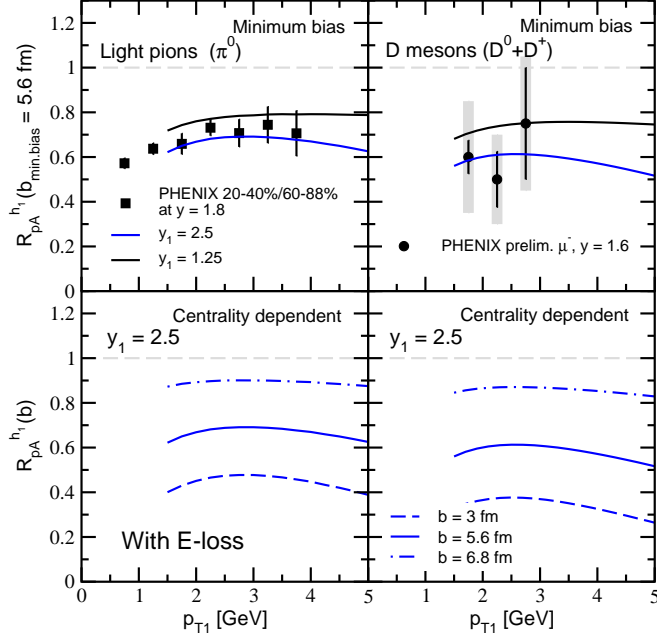


FIG. 14: Nuclear modification of single inclusive  $\pi^0$  (left panels) and  $D^0 + D^+$  mesons (right panels) in d+Au collisions at RHIC. The same rapidities and centralities as in Fig. 10 are shown. Energy loss is taken into account in the theoretical calculations.

function [25, 26] scattering on light quarks and gluons  $cg \rightarrow cg$ ,  $cq(\bar{q}) \rightarrow cq(\bar{q})$ . Our results for the mechanism of  $D$  meson production are readily testable at RHIC and LHC via charm quark triggered two particle measurements [31, 32]. It is a robust prediction of this approach that at  $p_{T2} < p_{T1}$  the  $D$  meson triggered away-side jet is dominated by hadrons from the fragmentation of light quarks and gluons. Only at transverse momenta  $p_{T2} \geq p_{T1}$  is the associated yield found to be dominated by  $D$  mesons. Such experimental measurements will be able to shed light on the partonic processes responsible for  $D$  meson production and also constrain the hardness of the non-perturbative heavy quark fragmentation functions [27]. Our results are also suggestive that inclusive heavy meson cross sections may be larger than the ones obtained in perturbative expansions that always treat  $c$  and  $b$  quarks as “heavy” [24].

In p(d)+A reactions we calculated and resummed the nuclear-enhanced coherent power corrections [12, 13] to single inclusive  $D$  meson production and  $D$  meson-triggered di-hadron yields. Improving upon our previous work [10], we established here the effect of the heavy quark mass on the power corrections and found it to be relatively small for charm quarks. We also extended the study of coherent multiple scattering to all  $s$ -,  $t$ - and  $u$ -channels. While forward rapidity at RHIC is dominated by DIS-like  $t$ -channel final-state interactions other kinematic domains and other particle production processes, such as the Drell-Yan, are controlled by different chan-

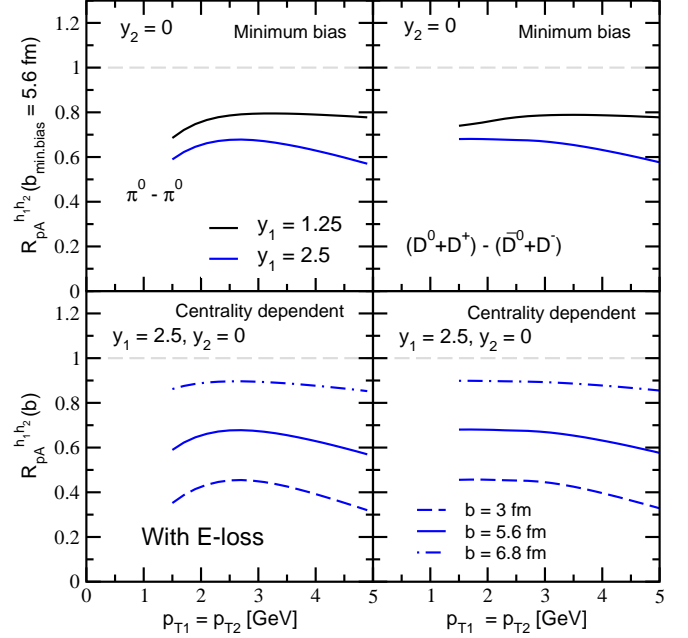


FIG. 15: Nuclear modification of  $\pi^0 - \pi^0$  di-hadron correlations (left panels) and  $(D^0 + D^+) - (\bar{D}^0 + \bar{D}^+)$  mesons correlations (right panels) in d+Au collisions at RHIC. The same rapidities and centralities as in Fig. 11 are shown. Energy loss is taken into account in the theoretical calculations.

nels. In this paper, by direct calculation, we demonstrated that *initial-state*  $s$ -channel multiple interactions lead to an enhancement in the cross sections in clear contrast to final-state suppression. We have thus further corroborated the conclusion that enhancement/suppression effects in reactions with nuclei are dynamically generated in the collision [5, 8, 10, 20, 21]. We find that they are not universal (are process dependent) and cannot be separated in the parton distribution or fragmentation functions.

Numerically, we found that dynamical high-twist shadowing can suppress single inclusive  $D$  meson production by as much as it does light hadrons. Similar results were obtained for di-hadron production with light and heavy quark triggers in the rapidity range  $y_1 = 1 - 4$  studied at RHIC. The nuclear modification at forward rapidity and small  $p_T \sim 1$  GeV can be substantial,  $\sim 30 - 50\%$ . At high  $p_T$ , however, it disappears quickly  $\propto 1/p_T^2$  and cannot fully explain the nuclear suppression measured in d+Au reactions by PHENIX [17, 36] and STAR [18]. Our calculations are fully constrained by existing DIS data [12] and provide an upper limit on nuclear modification from dynamical high-twist shadowing. Deviations between the calculations and the existing data are indicative of inelastic scattering in nuclei [22].

To determine the additional dynamical effects that lead to forward-backward hadron production asymmetry in proton-nucleus collisions in a model-independent way, we investigated low energy d+Au collisions [33] where coher-



ent scattering does not play a role. Suppression of forward rapidity hadrons, similar to that observed at RHIC, is found and is consistent with jet energy loss in cold nuclear matter. We have shown that, based on initial-state partonic implementation of energy loss [8] similar to the established incorporation of final-state  $\Delta E$  [5], the forward rapidity suppression can be described over the widest dynamic range in p(d)+A collisions accessible to perturbative QCD analysis. Specifically, we implemented radiative energy loss of the type derived by Bertsch and Gunion [19] and found that if the average parton loses  $\sim 10\%$  of its energy in minimum bias reactions with nuclei such as Au and Pb, this can explain the suppression of forward hadron production from SPS to RHIC. Inclusion of cold nuclear matter energy loss together with coherent power corrections results in suppression of both single inclusive hadron production and hadron triggered inclusive two particle yields (including  $D$  mesons and  $D\bar{D}$  pair production) which are fully consistent with the forward rapidity hadron attenuation measurements at RHIC [17, 18, 36].

The implication of such energy loss for extracting the scale of momentum transfer in cold nuclear matter merits further investigation. Of particular interest are analytic solutions for *initial*-state gluon bremsstrahlung, including coherence effects to all orders in the correlation between multiple scattering centers. In the future,

These can be studied numerically and implemented in the pQCD formalism with a degree of sophistication that will match the well-developed final-state energy loss phenomenology [5].

In summary, we have presented the first perturbative QCD calculation on heavy meson triggered di-hadron yields and showed how it can provide information on the  $D$  meson production mechanism and the non-perturbative fragmentation of heavy quarks. We identified the nuclear effects that dominate the cold nuclear matter attenuation of  $D$  meson and light hadron production at forward rapidities, which has drawn considerable interest in its own right. This work also provides the baseline for precision QGP tomography using heavy quarks as probes of the plasma away from midrapidity where new experimental capabilities at RHIC and the LHC are expected to become available.

### Acknowledgments

This research is supported in part by the US Department of Energy under Contract No. W-7405-ENG-3, Grant No. DE-FG02-87ER40371 and the J. Robert Oppenheimer Fellowship of the Los Alamos National Laboratory.

## APPENDIX A: FLAVOR CREATION AND FLAVOR EXCITATION DIAGRAMS

We emphasize that our need for the matrix elements calculated here is our interest in matching the  $m_c = 0$  charm quarks from the parton distribution functions to the  $m_c \neq 0$  in the final state. The internal heavy quark propagators are treated as massive.

The dominant mode of charm-anticharm di-jet production and subsequent fragmentation into  $D\bar{D}$  mesons comes

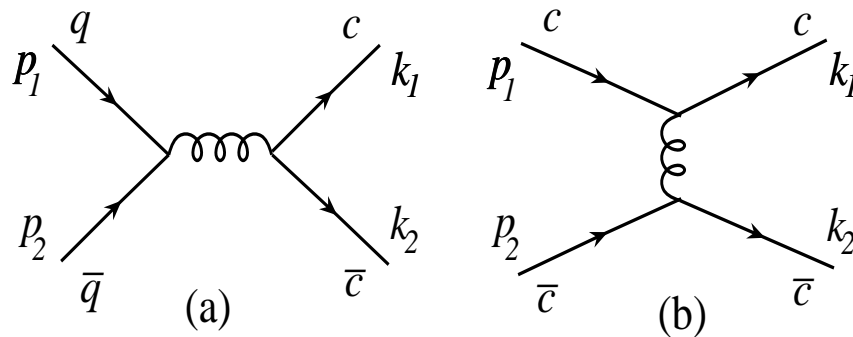


FIG. 16: (a) Light quark-antiquark annihilation into a massive  $c\bar{c}$  final state. (b)  $t$ -channel scattering contribution for the case of non-negligible initial (anti)charm parton distributions. Note that for  $c\bar{c} \rightarrow c\bar{c}$  both diagrams contribute. Time increases from left to right in all diagrams and arrows indicate momentum flow.

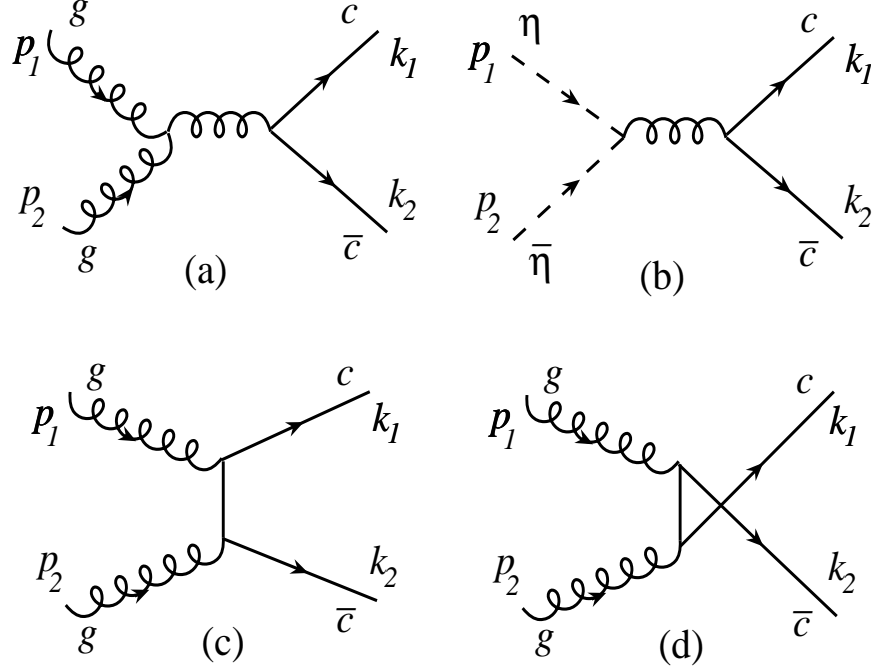


FIG. 17: (a) Gluon fusion via the  $s$ -channel into a  $c\bar{c}$  final state. (b) Ghost-antighost annihilation that cancels the contribution from the unphysical gluon polarization states in the covariant gauge. (c)  $t$ -channel and (d) the crossed  $u$ -channel charm exchange diagram.

from gluon fusion and light quark-antiquark annihilation. The  $c\bar{c}$  creation diagrams from  $q = (u, d, s)$  quarks are shown in Fig. 16(a). An additional  $t$ -channel scattering diagram contributes in Fig. 16(b) in the case of non-negligible (anti)charm distributions in the nucleon wave-function. In all figures the arrows indicate momentum flow. The matrix element corresponding to Fig. 16(a) reads:

$$i\mathcal{M}_{q\bar{q} \rightarrow c\bar{c}}^{(a)} = \bar{u}(k_1) (-ig_s \gamma^\mu T^a) v(k_2) \frac{-ig_{\mu\nu} \delta^{ab}}{(p_1 + p_2)^2 + i\epsilon} \bar{v}(p_2) (-ig_s \gamma^\nu T^b) u(p_1). \quad (\text{A1})$$

For identical initial- and final-state quark flavors, the  $t$ -channel must also be considered:

$$i\mathcal{M}_{c\bar{c} \rightarrow c\bar{c}}^{(b)} = -\bar{u}(k_1) (-ig_s \gamma^\mu T^a) u(p_1) \frac{-ig_{\mu\nu} \delta^{ab}}{(p_1 - k_1)^2 + i\epsilon} \bar{v}(p_2) (-ig_s \gamma^\nu T^b) v(k_2). \quad (\text{A2})$$

The relative “ $-$ ” between Eqs. (A1) and (A2) comes from Wick’s theorem. The dominant contribution to the  $c\bar{c}$  cross section comes from the diagrams with gluonic initial states:

$$i\mathcal{M}_{gg \rightarrow c\bar{c}}^{(a)} = \bar{u}(k_1) (-ig_s \gamma^\lambda T^c) v(k_2) \frac{-ig_{\lambda\lambda'}}{(p_1 + p_2)^2 + i\epsilon} (g_s f^{abc}) \left[ g^{\mu\nu} (p_1 - p_2)^{\lambda'} + g^{\nu\lambda'} (2p_2 + p_1)^\mu + g^{\lambda'\mu} (-2p_1 - p_2)^\nu \right] \epsilon_\mu^{\lambda_1}(p_1) \epsilon_\nu^{\lambda_2}(p_2), \quad (\text{A3})$$

$$i\mathcal{M}_{gg \rightarrow c\bar{c}}^{(c)} = \bar{u}(k_1) (-ig_s \gamma^\mu T^a) i \frac{\gamma \cdot (k_1 - p_1) + m_c}{(k_1 - p_1)^2 - m_c^2 + i\epsilon} (-ig_s \gamma^\nu T^b) v(k_2) \epsilon_\mu^{\lambda_1}(p_1) \epsilon_\nu^{\lambda_2}(p_2), \quad (\text{A4})$$

$$i\mathcal{M}_{gg \rightarrow c\bar{c}}^{(d)} = \bar{u}(k_1) (-ig_s \gamma^\nu T^b) i \frac{\gamma \cdot (p_1 - k_2) + m_c}{(p_1 - k_2)^2 - m_c^2 + i\epsilon} (-ig_s \gamma^\mu T^a) v(k_2) \epsilon_\mu^{\lambda_1}(p_1) \epsilon_\nu^{\lambda_2}(p_2). \quad (\text{A5})$$

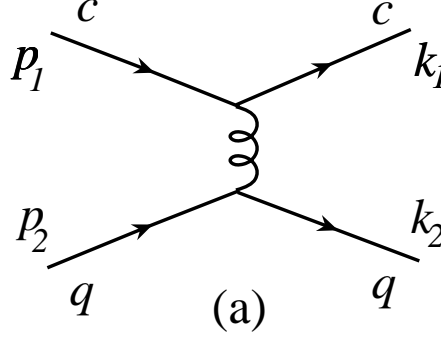


FIG. 18: (a) Heavy quark on light quark scattering via  $t$ -channel gluon exchange. Diagrams for scattering of anticharm and/or light antiquarks are similar.

In the covariant gauge used in this calculation, there are contributions at the cross section level coming from the unphysical gluon polarizations. The diagram  $\mathcal{M}^{(a)}$  in Fig. 16(a) is an example of where Fadeev-Popov ghost-antighost annihilation diagrams, two of them with  $\bar{\eta}$  and  $\eta$  interchanged, have to be taken into account:

$$i\mathcal{M}_{\bar{\eta}\eta \rightarrow c\bar{c}}^{(b)} = \bar{u}(k_1) (-ig_s \gamma^\mu T^b) v(k_2) \frac{-ig_{\mu\nu}}{(p_1 + p_2)^2 + i\epsilon} (g_s f^{abc}) (-p_1^\mu). \quad (\text{A6})$$

We recall that a closed ghost loop comes with a “ $-$ ” sign and the color factor is the same as in  $|\mathcal{M}^{(a)}|^2$ .

For the case of single inclusive  $D$  meson production, (anti)charm scattering on light quarks and gluons must also be included. We illustrate the calculation for quarks, as shown in Fig. 18. Results for antiquarks are similar. Only one diagram contributes to heavy on light quark scattering:

$$i\mathcal{M}_{cq \rightarrow cq}^{(a)} = -\bar{u}(k_1) (-ig_s \gamma^\mu T^a) u(p_1) \frac{-ig_{\mu\nu} \delta^{ab}}{(p_1 - k_1)^2 + i\epsilon} \bar{u}(k_2) (-ig_s \gamma^\nu T^b) u(p_2). \quad (\text{A7})$$

Figure 19 shows the contribution of charm quark scattering on gluons. For  $t$ -channel gluon exchange, the matrix element,  $\mathcal{M}^{(a)}$ , is:

$$i\mathcal{M}_{cg \rightarrow cg}^{(a)} = \bar{u}(k_1) (-ig_s \gamma^\lambda T^c) u(p_1) \frac{-ig_{\lambda\lambda'}}{(k_1 - p_1)^2 + i\epsilon} (g_s f^{abc}) \left[ g^{\mu\nu} (p_2 + k_2)^{\lambda'} + g^{\nu\lambda'} (p_2 - 2k_2)^\mu + g^{\lambda'\mu} (k_2 - 2p_2)^\nu \right] \epsilon_\mu^{\lambda_1} (p_2) \epsilon_\nu^{*\lambda_2} (k_2), \quad (\text{A8})$$

where the unphysical gluon polarizations are again canceled by the ghost contribution:

$$i\mathcal{M}_{cg \rightarrow cg}^{(b)} = \bar{u}(k_1) (-ig_s \gamma^\lambda T^c) u(p_1) \frac{-ig_{\lambda\lambda'}}{(k_1 - p_1)^2 + i\epsilon} (g_s f^{abc}) (-p_2)^{\lambda'}. \quad (\text{A9})$$

The other diagrams that contribute are  $u$ -channel and  $s$ -channel virtual quark exchange,  $\mathcal{M}^{(c)}$  and  $\mathcal{M}^{(d)}$  respectively, given for the example of charm by:

$$i\mathcal{M}_{cg \rightarrow cg}^{(c)} = \bar{u}(k_1) (-ig_s \gamma^\mu T^a) i \frac{\gamma \cdot (p_1 - k_2) + m_c}{(p_1 - k_2)^2 - m_c^2 + i\epsilon} (-ig_s \gamma^\nu T^b) u(p_1) \epsilon_\mu^{\lambda_1} (p_2) \epsilon_\nu^{*\lambda_2} (k_2), \quad (\text{A10})$$

$$i\mathcal{M}_{cg \rightarrow cg}^{(d)} = \bar{u}(k_1) (-ig_s \gamma^\nu T^a) i \frac{\gamma \cdot (k_1 + k_2) + m_c}{(k_1 + k_2)^2 - m_c^2 + i\epsilon} (-ig_s \gamma^\mu T^b) u(p_1) \epsilon_\mu^{\lambda_1} (p_2) \epsilon_\nu^{*\lambda_2} (k_2), \quad (\text{A11})$$

Next, we recall the definition of the Mandelstam invariants:

$$\begin{aligned} \hat{s} &= (p_1 + p_2)^2 = (k_1 + k_2)^2, \\ \hat{t} &= (p_1 - k_1)^2 = (p_2 - k_2)^2, \\ \hat{u} &= (p_1 - k_2)^2 = (p_2 - k_1)^2. \end{aligned} \quad (\text{A12})$$

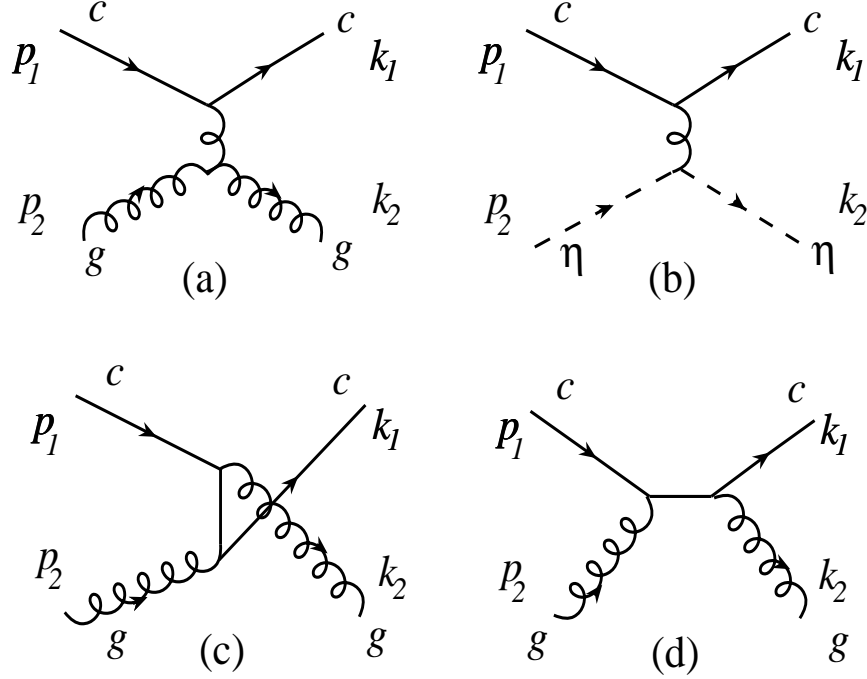


FIG. 19: (a) Charm quark on gluon scattering via  $t$ -channel gluon exchange. (b) Charm-ghost scattering that cancels the contribution from the unphysical gluon polarization states in the covariant gauge. (c) Charm quark on gluon scattering via virtual heavy quark exchange in the  $u$ -channel. (d) The corresponding  $s$ -channel diagram. Anticharm on gluon scattering is given by a similar set of diagrams.

In simplifying the result for the squared matrix elements, for charm-anticharm production we have  $\hat{s} + \hat{t} + \hat{u} = 2m_c^2$  and for charm on light parton scattering we have  $\hat{s} + \hat{t} + \hat{u} = m_c^2$ . We have taken all massless initial-state partons. The spin (polarization) and color averages  $\langle \dots \rangle$  are defined in the usual way:

$$\langle \dots \rangle_{\text{spin}} = \frac{1}{2} \sum_{s=\pm 1/2} \quad - \text{quarks}, \quad \langle \dots \rangle_{\text{polarization}} = \frac{1}{2} \sum_{\lambda=1,2} \quad - \text{gluons}, \quad (\text{A13})$$

$$\langle \dots \rangle_{\text{color}} = \frac{1}{N_c} \sum_{a=1 \dots N_c} \quad - \text{quarks}, \quad \langle \dots \rangle_{\text{color}} = \frac{1}{(N_c^2 - 1)} \sum_{a=1 \dots N_c^2 - 1} \quad - \text{gluons}, \quad (\text{A14})$$

where  $N_c = 3$  is the number of colors. Summation over the final-state spin (polarization) and color is understood.

In calculating the color factors we used factorization of the color algebra and the Lorentz structure in the Feynman graphs. A diagrammatic approach in non-Abelian gauge theories is employed in the calculation below. This is the same approach that was used in the evaluation of the significantly more involved color factors [20, 21] associated with medium-induced gluon bremsstrahlung. The calculation of the squared amplitudes, Eqs. (A1)-(A10) is straightforward though somewhat tedious in the presence of non-zero parton mass for final-state heavy quarks,  $\sum_{s=\pm 1/2} u^s(p) \bar{u}^s(p) = \gamma \cdot p + m$ ,  $\sum_{s=\pm 1/2} v^s(p) \bar{v}^s(p) = \gamma \cdot p - m$ . In the squared matrix elements given below, the color factors are separated in angle  $\langle \dots \rangle$  brackets and a “-” sign inside denotes a destructive color interference.

For light quark annihilation into a massive  $c\bar{c}$  final state:

$$\langle |\mathcal{M}_{q\bar{q} \rightarrow c\bar{c}}|^2 \rangle = \left\langle \frac{2}{9} \right\rangle \frac{2g_s^4}{\hat{s}^2} (t^2 + \hat{u}^2 + 4m_c^2 \hat{s} - 2m_c^4). \quad (\text{A15})$$

For charm quark-antiquark scattering by  $t$ -channel gluon exchange and  $s$ -channel annihilation into a massive  $c\bar{c}$  pair

the result is:

$$\begin{aligned} \langle |\mathcal{M}_{c\bar{c} \rightarrow c\bar{c}}|^2 \rangle &= \left\langle \frac{2}{9} \right\rangle \frac{2g_s^4}{\hat{s}^2} (\hat{t}^2 + \hat{u}^2 + 4m_c^2 \hat{s} - 2m_c^4) + \left\langle \frac{2}{9} \right\rangle \frac{2g_s^4}{\hat{t}^2} (\hat{s}^2 + \hat{u}^2 + 2m_c^2 \hat{t} - 3m_c^4) \\ &\quad + \left\langle -\frac{2}{27} \right\rangle \frac{4g_s^4}{\hat{s}\hat{t}} (\hat{u}^2 + m_c^2 \hat{s} - 2m_c^2 \hat{u} + m_c^4). \end{aligned} \quad (\text{A16})$$

Finally, the result for gluon fusion into a heavy charm-anticharm pair, which includes the corresponding  $t$ -channel and  $u$ -channel scattering, is:

$$\begin{aligned} \langle |\mathcal{M}_{gg \rightarrow c\bar{c}}|^2 \rangle &= -\left\langle \frac{3}{16} \right\rangle \frac{4g_s^4}{\hat{s}^2} (\hat{s}^2 - \hat{t}\hat{u} + m_c^2 \hat{s} + m_c^4) \\ &\quad + \left\langle \frac{1}{12} \right\rangle \frac{2g_s^4}{(\hat{t} - m_c^2)^2} (\hat{t}\hat{u} + m_c^2 \hat{s} - 2m_c^2 \hat{t} - 3m_c^4) + \left\langle \frac{1}{12} \right\rangle \frac{2g_s^4}{(\hat{u} - m_c^2)^2} (\hat{t}\hat{u} + m_c^2 \hat{s} - 2m_c^2 \hat{u} - 3m_c^4) \\ &\quad - \left\langle \frac{3}{32} \right\rangle \frac{4g_s^4}{\hat{s}(\hat{t} - m_c^2)} (\hat{t}^2 + m_c^2 \hat{s} - 2m_c^2 \hat{t} + m_c^4) + \left\langle -\frac{3}{32} \right\rangle \frac{4g_s^4}{\hat{s}(\hat{u} - m_c^2)} (\hat{u}^2 + m_c^2 \hat{s} - 2m_c^2 \hat{u} + m_c^4) \\ &\quad + \left\langle -\frac{1}{96} \right\rangle \frac{4g_s^4}{(\hat{t} - m_c^2)(\hat{u} - m_c^2)} (m_c^2 \hat{s} - 4m_c^4). \end{aligned} \quad (\text{A17})$$

We turn next to the additional contributions to single inclusive charm production. The scattering of heavy on light (anti)quarks via  $t$ -channel gluon exchange yields:

$$\langle |\mathcal{M}_{cq \rightarrow cq}|^2 \rangle = \left\langle \frac{2}{9} \right\rangle \frac{2g_s^4}{\hat{t}^2} (\hat{s}^2 + \hat{u}^2 + m_c^2 \hat{t} - m_c^4). \quad (\text{A18})$$

For the case of charm quarks scattering on gluons, we obtain:

$$\begin{aligned} \langle |\mathcal{M}_{cg \rightarrow cg}|^2 \rangle &= +\left\langle \frac{1}{2} \right\rangle \frac{g_s^4}{\hat{t}^2} (4\hat{t}^2 - 4\hat{s}\hat{u} - m_c^2 \hat{s} - 3m_c^2 \hat{t} - m_c^4) \\ &\quad - \left\langle \frac{2}{9} \right\rangle \frac{2g_s^4}{(\hat{u} - m_c^2)^2} (\hat{s}\hat{u} + 2m_c^2 \hat{u} - m_c^2 \hat{s}) - \left\langle \frac{2}{9} \right\rangle \frac{2g_s^4}{(\hat{s} - m_c^2)^2} (\hat{s}\hat{u} + 2m_c^2 \hat{s} - m_c^2 \hat{u}) \\ &\quad - \left\langle -\frac{1}{4} \right\rangle \frac{2g_s^4}{\hat{t}(\hat{u} - m_c^2)} (2\hat{u}^2 - 5m_c^2 \hat{u} + m_c^2 \hat{t} - m_c^4) + \left\langle \frac{1}{4} \right\rangle \frac{2g_s^4}{\hat{t}(\hat{s} - m_c^2)} (2\hat{s}^2 - 5m_c^2 \hat{s} + m_c^2 \hat{t} - m_c^4) \\ &\quad + \left\langle -\frac{1}{36} \right\rangle \frac{4g_s^4}{(\hat{s} - m_c^2)(\hat{u} - m_c^2)} (m_c^4 - m_c^2 \hat{t}). \end{aligned} \quad (\text{A19})$$

We can partially check all results by taking the massless,  $m_c \rightarrow 0$ , limit. If we denote by  $(\bar{q})q$  the light  $u, d, s$  (anti)quarks, we recover the familiar form of the squared matrix elements:

$$\lim_{m_c \rightarrow 0} \langle |\mathcal{M}_{q\bar{q} \rightarrow c\bar{c}}|^2 \rangle = \langle |\mathcal{M}_{q\bar{q} \rightarrow q'\bar{q}'}|^2 \rangle = \frac{4g_s^4}{9} \left( \frac{\hat{t}^2 + \hat{u}^2}{\hat{s}^2} \right), \quad (\text{A20})$$

$$\lim_{m_c \rightarrow 0} \langle |\mathcal{M}_{c\bar{c} \rightarrow c\bar{c}}|^2 \rangle = \langle |\mathcal{M}_{q\bar{q} \rightarrow q\bar{q}}|^2 \rangle = \frac{4g_s^4}{9} \left( \frac{\hat{t}^2 + \hat{u}^2}{\hat{s}^2} + \frac{\hat{s}^2 + \hat{u}^2}{\hat{t}^2} - \frac{2}{3} \frac{\hat{u}^2}{\hat{s}\hat{t}} \right), \quad (\text{A21})$$

$$\lim_{m_c \rightarrow 0} \langle |\mathcal{M}_{gg \rightarrow c\bar{c}}|^2 \rangle = \langle |\mathcal{M}_{gg \rightarrow q\bar{q}}|^2 \rangle = \frac{3g_s^4}{8} \left( \frac{\hat{t}^2 + \hat{u}^2}{\hat{s}^2} \right) \left( \frac{4}{9} \frac{\hat{s}^2}{\hat{t}\hat{u}} - 1 \right). \quad (\text{A22})$$

$$\lim_{m_c \rightarrow 0} \langle |\mathcal{M}_{cq \rightarrow cq}|^2 \rangle = \langle |\mathcal{M}_{q\bar{q}' \rightarrow q\bar{q}'}|^2 \rangle = \frac{4g_s^4}{9} \left( \frac{\hat{s}^2 + \hat{u}^2}{\hat{t}^2} \right), \quad (\text{A23})$$

$$\lim_{m_c \rightarrow 0} \langle |\mathcal{M}_{cg \rightarrow cg}|^2 \rangle = \langle |\mathcal{M}_{qg \rightarrow qg}|^2 \rangle = g_s^4 \left[ 2 \left( 1 - \frac{\hat{s}\hat{u}}{\hat{t}^2} \right) - \frac{4}{9} \left( \frac{\hat{s}}{\hat{u}} + \frac{\hat{u}}{\hat{s}} \right) - 1 \right]. \quad (\text{A24})$$

For comparison, see Ref. [2].



## APPENDIX B: FACTORIZATION APPROACH TO COHERENT MULTIPLE SCATTERING

In proton-nucleus reactions at RHIC the negative lightcone direction is assigned to the nucleus. Thus, the proton has momentum  $p_A = [p_A^+, 0, 0_\perp]$  and the nucleus has momentum  $P_B = [0, P_B^-, 0_\perp]$ . We again remind the reader that “ $B$ ” and “ $b$ ” are just labels for the target nucleus with mass number  $A$ . For example,  $p_B \approx P_B/A$  is the momentum per nucleon. Here, we neglect the Fermi momentum and the binding energy of the nucleons in the nucleus. For momentum exchange  $q^\mu = (p_c/z_1 - x_a p_A)^\mu$  we rotate to a frame where parton “ $d$ ” interacts head on with the remnants of the nucleus. Let  $\bar{n}^\mu = [1, 0, 0_\perp]$ ,  $n^\mu = [0, 1, 0_\perp]$  specify the “+” and “−” lightcone directions, respectively. In the equivalent Breit frame

$$q^\mu = -\tilde{x}_b p_B^- n + \frac{-\hat{t}}{2\tilde{x}_b p_B^-} \bar{n}, \quad q^2 = \hat{t}. \quad (\text{B1})$$

Here,  $\tilde{x}_b$  can be derived from the requirement that when the scattered parton “ $d$ ” of momentum  $x p_B^- n^\mu + q^\mu$  is on shell. The  $t = \infty$  cut constrains the momentum fraction from the nucleus to the known solution, Eq. (6),

$$\delta((q + x p_B)^2 - m_d^2) \propto \delta(x - x_b) \quad \Rightarrow \quad \tilde{x}_b = \frac{x_b}{1 + m_d^2/(-\hat{t})}. \quad (\text{B2})$$

We note that above, “ $d$ ” is the label, not the flavor, of the outgoing parton. In particular when “ $d$ ” is a  $c$  quark we will have  $m_d = m_c = 1.3$  GeV.

Under the standard convention about the “+” and “−” lightcone directions at RHIC, it is convenient to use the  $A \cdot \bar{n} = A^- = 0$  gauge. Such a choice does not affect any of the physical quantities that appear in the final result. For example, the parton distributions, the scale of higher twist and the hard scattering partonic cross sections and the Mandelstam variables are all *individually* boost and gauge invariant. We consider the final-state interactions of parton “ $d$ ” with the gluons from the nucleus with  $A^\mu(y_i^+) \approx A^\perp(y_i^+)$  shown in Fig. 20. Using

$$F^{\perp-}(y_i^+) = \frac{\partial A^\perp(y_i^+)}{\partial y_i^+} - \frac{\partial A^-(y_i^+)}{\partial y_i^\perp} + ig [A^\perp(y_i^+), A^-(y_i^+)] = \frac{\partial A^\perp(y_i^+)}{\partial y_i^+}, \quad (\text{B3})$$

the gluon fields can be represented as components of the field strength tensor. The initial-state parton carries momentum fraction  $x_0$  and  $2n$  gluons carry momentum fractions  $\tilde{x}_i - x_{i-1}$ , at positions  $\tilde{y}_i^+$ , and fractions  $x_i - \tilde{x}_i$ , at positions  $y_i^+$ , of the momenta  $p_B = P_B/A$  of their corresponding nucleons. Such choice of the momentum transfers ensures the flow indicated in Fig. 20 and a simple representation of the momentum fraction in each of the propagators

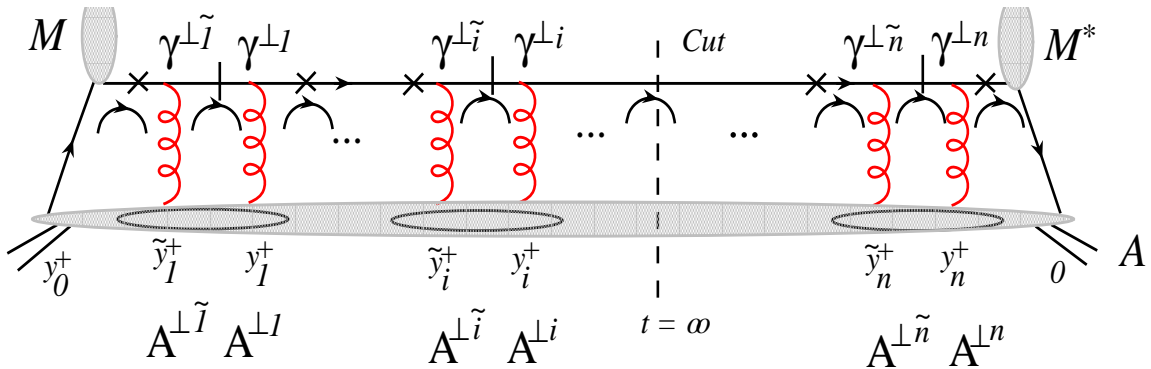


FIG. 20: Multiple coherent scattering of the outgoing partons in proton-nucleus reactions in the  $t$ -channel. We have denoted by  $\times \rightarrow$  and  $\vdash \rightarrow$  the long distance and contact propagators, respectively. We have indicated the lightcone positions, e.g.  $y_i^+$ . Arcs show the momentum routing. Gluons are dominated by their transverse components and the fields, e.g.  $A^{\perp i}(y_i^+)$ , are shown before the conversion to the field strength tensor and before the factorization of the color and Lorentz indexes.

along the scattered parton line. The part of the diagram associated with the non-perturbative matrix element reads:

$$\begin{aligned}
& \int dx_0 \int \frac{dy_0^+}{2\pi} e^{ix_0 p_B^- y_0^+} \left[ \prod_{i=1}^n \int d\tilde{x}_i dx_i \int \frac{d\tilde{y}_i^+ p_B^-}{2\pi} \frac{dy_i^+ p_B^-}{2\pi} e^{i(\tilde{x}_i - x_{i-1}) p_B^- \tilde{y}_i^+} e^{i(x_i - \tilde{x}_i) p_B^- y_i^+} \right] \\
& \quad \times \left\langle P_B \left| \mathcal{O}^{init} A^\perp(y_n^+) A^\perp(\tilde{y}_n^+) \cdots A^\perp(y_i^+) A^\perp(\tilde{y}_i^+) \cdots A^\perp(y_1^+) A^\perp(\tilde{y}_1^+) \right| P_B \right\rangle \\
& = \int dx_0 \int \frac{dy_0^+}{2\pi} e^{ix_0 p_B^- y_0^+} \left[ \prod_{i=1}^n \int d\tilde{x}_i dx_i \int \frac{d\tilde{y}_i^+}{2\pi} \frac{dy_i^+}{2\pi} \frac{e^{i(\tilde{x}_i - x_{i-1}) p_B^- \tilde{y}_i^+}}{i(\tilde{x}_i - x_{i-1} - i\epsilon)} \frac{e^{i(x_i - \tilde{x}_i) p_B^- y_i^+}}{i(x_i - \tilde{x}_i - i\epsilon)} \right] \\
& \quad \times \left\langle P_B \left| \mathcal{O}^{init} F^{-\perp}(y_n^+) F_\perp^-(\tilde{y}_n^+) \cdots F^{-\perp}(y_i^+) F_\perp^-(\tilde{y}_i^+) \cdots F^{-\perp}(y_1^+) F_\perp^-(\tilde{y}_1^+) \right| P_B \right\rangle. \quad (B4)
\end{aligned}$$

In Eq. (B4) we have carried out an integration by parts assuming that the gluon fields vanish sufficiently fast at  $|y_i^+| \rightarrow \infty$ ,  $|\tilde{y}_i^+| \rightarrow \infty$ . The choice of  $-i\epsilon$  is convenient for guiding the evaluation of the remaining momentum fraction integrals [12] but can be verified by carrying out twist-4 calculations in the lightcone and covariant gauges and comparing the final result. Depending on the type of initial-state parton, the operator

$$\mathcal{O}^{quark} = \bar{\psi}(0) \frac{\gamma^-}{2} \psi(y_0^+), \quad \mathcal{O}^{gluon} = \frac{1}{x_0 p_B^-} F^{-\perp}(0) F_\perp^-(y_0^+). \quad (B5)$$

To factorize the twist-2 +  $2n$  non-perturbative matrix element we need to decouple the color and Lorentz indexes, which are not shown explicitly in the equation above. We use Fiertz transformations and identify the numerical factors associated with the diagonal terms that do not change the quantum number, for example color, of the parton after a pairwise gluon exchange. We obtain  $-1/2$  for the Lorentz part and  $1/2N_c = 1/6$  or  $N_c/(N_c^2 - 1) = 3/8$  for a final-state interacting quark or gluon, respectively. After this factorization of indexes, we obtain pairwise contractions  $F^{-\perp i}(\tilde{y}_i^+) F_\perp^-(y_i^+)$  in the non-perturbative matrix element, where average over color is implicit, and  $-\frac{1}{2}(g_\perp)_{\tilde{i}i} \gamma^{\perp \tilde{i}} \cdots \gamma^{\perp i}$  in the hard scattering matrix element, which we can evaluate perturbatively in QCD.

Let us now focus on the propagator structure along the outgoing parton “ $d$ ”. For definiteness we consider a heavy quark. With *net* momentum transfer  $x_i p_B^-$  from the nucleus, the quark propagator can be represented as follows

$$\mathcal{D}(x_i, x_b, -\hat{t}, m_d) = i \left( \frac{\tilde{x}_b}{-\hat{t}} \right) p_B^- \gamma^+ + i \left( \frac{\tilde{x}_b}{-\hat{t}} \right) \frac{(\gamma \cdot \tilde{p} + m_d)}{x_i - x_b + i\epsilon}. \quad (B6)$$

In Eq. (B6) the  $x_i$ -independent vector  $\tilde{p}$  is on shell

$$\tilde{p}^\mu = (x_b - \tilde{x}_b) p_B^- n^\mu + \frac{-\hat{t}}{2\tilde{x}_b p_B^-} \bar{n}^\mu, \quad \tilde{p}^2 = m_d^2. \quad (B7)$$

We emphasize that the propagators along the final-state parton line have two distinct parts [12, 13]. The first one does not have a pole in terms of the yet undetermined momentum  $x_i p_B^-$ . In the Fourier space of the conjugate variable  $y^+$ , the interactions that such a propagator separates can be collapsed to a single point,  $\propto \delta(\Delta y^+)$ . Therefore, the short-distance two-gluon exchange can be evaluated within the *same* nucleon state. On the other hand, the second part of the propagator has a pole at  $x_i = x_b$ , which puts the propagating parton on shell and ensures a long lifetime. In Fourier space, the subsequent interactions separated by this propagator  $\propto \theta(\Delta y^+)$  can be long distance and are only limited by the nuclear size  $\sim r_0 A^{1/3}$ , where  $A$  is the nuclear target mass number. In our notation the  $t = \infty$  on-shell cut line through parton “ $d$ ” reads

$$\mathcal{C}(x_i, x_b, -\hat{t}, m_d) = 2\pi \left( \frac{\tilde{x}_b}{-\hat{t}} \right) (\tilde{p} \cdot \gamma + m_d) \delta(x_i - x_b). \quad (B8)$$

Naively, the sequence of propagators separated by the  $\gamma^\perp$  matrices may yield an exponentially large number of terms per single digram, similar to the one in Fig. 20. However, using the equations of motion for a massive particle, the commutation relations for the Dirac algebra and  $(\gamma^+)^2 = (\gamma^-)^2 = 0$ , we can simplify a typical sequence of propagators along scattered parton “ $d$ ” line as follows:

$$\begin{aligned}
& \cdots (\tilde{p} \cdot \gamma + m_d) \left[ \frac{g_s^2}{2N_c} \left( -\frac{1}{2} (g_\perp)_{i\tilde{i}} \right) \left( \frac{\tilde{x}_b}{-\hat{t}} \right)^2 \gamma^{\perp i} \left( p_B^- \gamma^+ + \frac{\gamma \cdot \tilde{p} + m_d}{\tilde{x}_i - x_b + i\epsilon} \right) \gamma^{\perp \tilde{i}} \left( p_B^- \gamma^+ + \frac{\gamma \cdot \tilde{p} + m_d}{x_{i-1} - x_b + i\epsilon} \right) \right] \cdots \\
& = \cdots (\tilde{p} \cdot \gamma + m_d) \left[ \frac{2\pi\alpha_s}{3} \left( \frac{\tilde{x}_b}{-\hat{t}} \right) \frac{\gamma^+ \gamma^-}{2} \frac{1}{x_{i-1} - x_b + i\epsilon} \right] \cdots \quad (B9)
\end{aligned}$$

where the boundary condition is set by the cut, Eq. (B8), and we have taken into account that the subsequent scattering has similar propagator structure. This is the first significant simplification, which makes it possible to calculate and resum the multiple final-state interactions of the struck parton.

The second important simplification comes from a model [12] for the high-twist matrix elements in Eq. (B4). The natural long and short distance separation of soft gluon interactions along the trajectory of the struck parton justifies the decomposition of the multi-local, multi-parton, non-perturbative matrix element in Eq. (B4) in a diagonal basis of individual nucleon states. We focus on the QCD aspects of the calculation and not the ones related to the nuclear structure. To illustrate our idea, we adopt a simplified model of a nucleus of constant lab frame number density:

$$\rho(r) = \frac{A}{V} = \frac{3}{4\pi r_0^3}, \quad (\text{B10})$$

where  $r_0 = 1.2$  fm is the nucleon radius. Each nucleon carries an equal fraction of the momentum of the nucleus,  $p_B \approx P_B/A$ , an approximation which is valid so long as the energy per nucleon is significantly larger than the binding energy,  $\epsilon \simeq 8$  MeV, and the momentum per nucleon is significantly larger than the Fermi momentum,  $k_F \approx 250$  MeV. If this condition is violated, the off-diagonal elements in a density matrix that represent the correlation between different nucleons might contribute significantly. With the normalization of the momentum states  $\langle p' | p \rangle = 2E_p(2\pi)^3 \delta^3(\vec{p} - \vec{p}')$ , the decomposition of the matrix element reads:

$$\begin{aligned} \left\langle P_B \left| \mathcal{O}^{init} \prod_{i=1}^n F^{-\perp}(y_i^+) F_{\perp}^-(\tilde{y}_i^+) \right| P_B \right\rangle &\approx A \langle p_B | \mathcal{O}^{init} | p_B \rangle \prod_{i=1}^n \frac{\rho(r)}{2E_{p_B}} \langle p_B | F^{-\perp}(y_i^+) F_{\perp}^-(\tilde{y}_i^+) | p_B \rangle \\ &= A \langle p_B | \mathcal{O}^{init} | p_B \rangle \prod_{i=1}^n \frac{3}{8\pi r_0^3 m_N} \langle p_B | F^{-\perp}(y_i^+) F_{\perp}^-(\tilde{y}_i^+) | p_B \rangle. \end{aligned} \quad (\text{B11})$$

From Eq. (B11) it follows that, in the absence of final-state coherent interactions, i.e. neglecting the  $\prod_{i=1}^n$  two-gluon correlations, the minimum bias, inclusive, deeply inelastic scattering structure functions, and the minimum bias differential hadron production cross section in proton-nucleus reactions, both scale with the number of the nucleons,  $A$ , in the nucleus. The expectation value of the bilocal quark or gluon operator  $\mathcal{O}^{init}$  enters the definition of the leading-twist quark parton distribution function in the nucleon and is always present as a first term in the twist expansion series.

Next, we carry out the integrations  $\prod_{i=1}^n \int d\tilde{x}_i dx_i$ . To determine the scale of high-twist corrections per nucleon, we recall that the integration over the single pole  $\tilde{x}_i^+$  in Eq. (B4) yields terms proportional to  $2\pi \theta(y_i^+ > \tilde{y}_i^+)$  and  $2\pi \theta(y_i^+ < \tilde{y}_i^+)$ . If the two gluon exchange is to the left of the  $t = \infty$  cut we keep the term  $\propto \theta(y_i^+ > \tilde{y}_i^+)$  and if the two gluon exchange is to the right of the  $t = \infty$  cut, we keep the term  $\propto \theta(y_i^+ < \tilde{y}_i^+)$ . This ensures that time grows toward  $t = \infty$  and that we keep the dominant nuclear-size-enhanced contribution. Inserting  $1 = \exp(i0 p_B^- \tilde{y}^+)$  we identify

$$(2\pi) \int \frac{\tilde{y}_i^+}{2\pi} e^{i0 p_B^- \tilde{y}^+} \frac{1}{p_B} \langle p_B | F_{\perp}^-(y_i^+) F^{-\perp}(\tilde{y}_i^+) | p_B \rangle \theta(y_i^+ > \text{ or } < \tilde{y}_i^+) = (2\pi) \lim_{x \rightarrow 0} \frac{1}{2} x G(x) \quad (\text{B12})$$

by direct comparison with the definition of the parton distribution functions [12]. Note that the lightcone positions  $y_i^+$ ,  $\tilde{y}_i^+$  can always be shifted due to translational invariance. The  $\theta$ -function yields a factor of 1/2 which can be thought of alternatively as arising from the symmetry in the legs of the two-gluon ladder at the interaction point. We emphasize that the scale of high-twist corrections depends on the soft  $x \rightarrow 0$  limit of the gluon momentum fraction in the nucleon. While finite resolution effects may alter this result to some small but finite value, this is the value of *neither* the Bjorken  $x$  *nor* the momentum fraction fixed by the hard scattering in hadronic reactions, Eq. (6). As emphasized below Eq. (2), we explicitly keep track of the  $A^{n/3}$  enhancement of the multiple soft scattering. We will show below that taking all possible cuts in a diagram with  $n$  2-gluon ladders gives contribution  $\propto (1/n!) A^{n/3}$ . We first identify the prefactors associated with such an exponentiating series. A dimensionless equivalent of an average path length of a struck parton through the nucleus is given by

$$\left\langle \int dy_i^+ p_B^- \theta(y_i^+) \right\rangle_{\text{Volume}} = \frac{3}{4} m_N r_0 A^{1/3}, \quad (\text{B13})$$

where the  $\langle \dots \rangle_{\text{Volume}}$  is carried out for uniform density, Eq. (B10). In a sequence of interactions where the two-gluon ladder contribution does not vanish, the  $\gamma^+ \gamma^- / 2$  matrices give a numerical factor of unity; for example,  $\text{Tr } \gamma^- (\gamma^+ \gamma^- / 2)^n \gamma^+ \dots = \text{Tr } \gamma^- \gamma^+ \dots$ . Collecting all factor from Eqs. (B9), (B11) and (B12), we obtain the parameter that controls the strength of the high-twist corrections on a single nucleon ( $A=1$ ) [10, 12, 13]

$$\xi^2 = \left( \frac{2\pi\alpha_s}{3} \right) \left( \frac{3}{8\pi r_0^3 m_N} \right) \left( \frac{3m_N r_0}{4} \right) \left( (2\pi) \lim_{x \rightarrow 0} \frac{1}{2} x G(x) \right) = \frac{3\pi\alpha_s}{8r_0^2} \lim_{x \rightarrow 0} \frac{1}{2} x G(x). \quad (\text{B14})$$

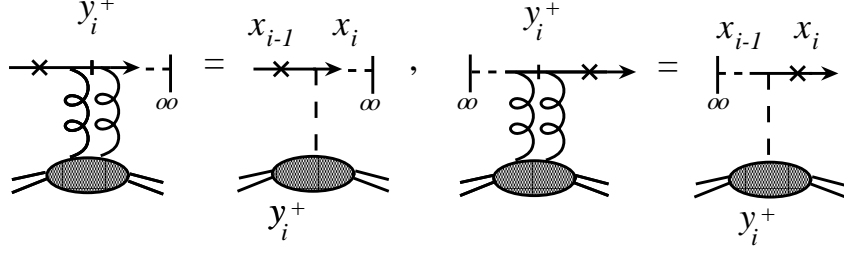


FIG. 21: Reduced Feynman diagram to the left and right of the  $t = \infty$  cut. The Feynman rules for the effective scalar interaction are given in Eqs. (B15) and (B16).

As we mentioned above, this does not include the  $A^{1/3}$  nuclear size enhancement, nor the derived factor of  $1/n!$  which can be intuitively understood from path ordered interactions [20].

It is useful to define effective Feynman rules, corresponding to the diagrams shown in Fig. 21, for the final-state soft scattering of the struck parton:

$$\tilde{x}_b \left( \frac{\xi^2}{-\hat{t}} \right) \int \frac{d\lambda_i}{2\pi} \frac{e^{i(x_i - x_{i-1})\lambda_i}}{x_i - x_{i-1} - i\epsilon} \frac{-i}{x_{i-1} - x_b + i\epsilon} \quad \text{left of } t = \infty, \quad (\text{B15})$$

$$\tilde{x}_b \left( \frac{\xi^2}{-\hat{t}} \right) \int \frac{d\lambda_i}{2\pi} \frac{e^{i(x_i - x_{i-1})\lambda_i}}{x_i - x_{i-1} - i\epsilon} \frac{-i}{x_i - x_b - i\epsilon} \quad \text{right of } t = \infty. \quad (\text{B16})$$

In Eqs. (B15) and (B16) we introduced the notation  $\lambda_i = p_B^- y_i^+$ . The difference from our result for DIS, given in Ref. [12], is that we have already performed the density matrix decomposition of the high-twist matrix element. Here,  $\tilde{x}_b$  replaces  $x_B$  and depends on the heavy quark mass, and  $Q^2 \rightarrow -\hat{t}$ . Numerical factors, including the contribution to the non-vanishing traces from the  $\gamma$ -matrices, are collected in the scale of higher twist,  $\xi^2$ , Eq. (B14).

The last part remaining is to demonstrate that the dimensionless integrals can be performed yielding the claimed  $A^{1/3}$  amplification of the higher-twist contribution through the exponentiation of the power series. The twist-2 +  $2n$  term reads:

$$\sum_{i=0}^n \int dx_0 dx_1 \cdots dx_n \int \frac{d\lambda_0}{2\pi} \frac{d\lambda_1}{2\pi} \cdots \frac{d\lambda_n}{2\pi} e^{ix_0\lambda_0} \frac{1}{p_B^-} \langle p_B | \mathcal{O}^{init} | p_B \rangle \\ \times \prod_{j=1}^i \frac{e^{i(x_j - x_{j-1})\lambda_j}}{x_{j-1} - x_b + i\epsilon} \frac{-i}{x_j - x_{j-1} - i\epsilon} \delta(x_i - x_b) \prod_{k=i+1}^n \frac{e^{i(x_k - x_{k-1})\lambda_k}}{x_k - x_b - i\epsilon} \frac{-i}{x_k - x_{k-1} - i\epsilon}. \quad (\text{B17})$$

In Eq. (B17), the appearance of  $1/p_B^-$  is associated with the conversion of  $\tilde{y}_0^+$  to  $\lambda_0$ . There may also be an additional function,  $H(x_0)$ , which contains smooth  $x_0$  dependence. The  $n = 0$  first term corresponds to there being no final-state interactions.

The integrals to the left and right of the  $t = \infty$  cut, which sets  $x_i = x_b$ , are taken independently. The integrals over the  $x_j, x_k$  poles can be carried out by closing the contour in the upper or lower half plane. We note that we have multiple poles. These produce  $\theta$ -functions which lead path ordering of the  $d\lambda_\alpha$  integration and powers of  $\lambda_\alpha - \lambda_\beta$ . Carrying out the  $\int d\lambda_1 \cdots d\lambda_n$ , we find

$$\int \frac{d\lambda_0}{2\pi} e^{ix_b\lambda_0} \frac{1}{p_B^-} \langle p_B | \mathcal{O}^{init} | p_B \rangle \sum_{i=0}^n \frac{i^i}{i!} \left[ -\frac{1}{2}(\Lambda - \lambda_0)^2 \right]^i \frac{i^{n-i}}{(n-i)!} \left[ \frac{1}{2}(\Lambda)^2 \right]^{n-i} \\ \approx \int \frac{d\lambda_0}{2\pi} e^{ix_b\lambda_0} \frac{1}{p_B^-} \langle p_B | \mathcal{O}^{init} | p_B \rangle \frac{1}{n!} (i\Lambda\lambda_0)^n = \frac{\Lambda^n}{n!} \frac{d^n}{dx_b^n} \left[ \int \frac{dy_0^+}{2\pi} e^{ix_b p_B^- y_0^+} \langle p_B | \mathcal{O}^{init} | p_B \rangle \right]. \quad (\text{B18})$$

In Eq. (B18),  $\Lambda = A^{1/3}\lambda_0$  and we have dropped a term  $\mathcal{O}(\lambda_0^2/2)$  which is suppressed by the large  $A^{1/3}$  nuclear size relative to  $\Lambda\lambda_0$ . In the presence of an additional function of  $x_0$ , for example  $H(x_0) = |\mathcal{M}_{ab \rightarrow cd}|^2/x_0$ , the multiple

poles to the left of the  $t = \infty$  cut lead to a series of derivatives on  $H(x_0)$ . The result for the modified Eq. (B17), where we have also included the  $(\tilde{x}_b \xi^2 / (-\hat{t}))^n$  power dependence, reads:

$$\begin{aligned} & \sum_{i=0}^n \left( \tilde{x}_b \frac{\xi^2}{-\hat{t}} \right)^n \int dx_0 dx_1 \cdots dx_n \int \frac{d\lambda_0}{2\pi} \frac{d\lambda_1}{2\pi} \cdots \frac{d\lambda_n}{2\pi} e^{ix_0 \lambda_0} \frac{1}{p_B} \langle p_B | \mathcal{O}^{init} | p_B \rangle H(x_0) \\ & \times \prod_{j=1}^i \frac{e^{i(x_j - x_{j-1})\lambda_j}}{x_{j-1} - x_b + i\epsilon} \frac{-i}{x_j - x_{j-1} - i\epsilon} \delta(x_i - x_b) \prod_{k=i+1}^n \frac{e^{i(x_k - x_{k-1})\lambda_k}}{x_k - x_b - i\epsilon} \frac{-i}{x_k - x_{k-1} - i\epsilon} \\ & \approx \frac{1}{n!} \left( \tilde{x}_b \frac{\xi^2 A^{1/3}}{-\hat{t}} \right)^n \frac{d^n}{dx_b^n} \left[ H(x_b) \int \frac{dy_0^+}{2\pi} e^{ix_b p_B^- y_0^+} \langle p_B | \mathcal{O}^{init} | p_B \rangle \right]. \end{aligned} \quad (\text{B19})$$

Note that all infrared singularities, naively present on the hard part, give a finite contribution after taking all possible cuts in the diagram, Fig. 20.

In studying the modification to the differential cross sections due to nuclear-enhanced power corrections, we can either take the scale defined in Eq. (B14) amplified by the nuclear size  $\propto A^{1/3}$  and a similar effect for the proton with  $A = 1$ , or assume that, for the case of the “elementary” nucleon, high-twist effects have been taken into account in the PDFs and additional interactions in the nucleus are  $\propto A^{1/3} - 1$ . The extraction of the scale of power corrections,  $\xi^2 = 0.09 - 0.12 \text{ GeV}^2$ , for quark scattering, from comparison to the shadowing in the nuclear structure function  $F_2^A(x, Q^2)$  [12], was performed using the second assumption. Improved analysis may yield somewhat different values for  $\xi^2$ . Finally, we recall that in the case of final-state gluon scattering, the color singlet coupling,  $N_c/(N_c^2 - 1) = 3/8$ , amplifies the scale of higher-twist effects by a factor of  $C_A/C_F = 9/4$  [10].

To complete the summation of all-twist, nuclear-enhanced power corrections, we identify the additional function  $H(x_b) = |M_{ab \rightarrow cd}|^2 / x_b$  from Eqs. (7) and (12). In Eq. (B17), it multiplies the leading-twist parton distribution  $\phi_{b/N}(x_b)$ . Thus, if we define [10]  $F_{ab \rightarrow cd}(x_b) = \phi_{b/N}(x_b) |M_{ab \rightarrow cd}|^2 / x_b$ . Implementing the normalization to no nuclear effect on a single nucleon as follows,  $A^{1/3} \rightarrow A^{1/3} - 1$ , and having allowed for both massless and massive partons (quarks or gluons) we find:

$$\begin{aligned} F_{ab \rightarrow cd}(x_b) & \Rightarrow \sum_{n=0}^{\infty} \frac{1}{n!} \left( \tilde{x}_b \frac{\xi^2 (A^{1/3} - 1)}{-\hat{t}} \right)^n \frac{d^n}{dx_b^n} F_{ab \rightarrow cd}(x_b) = \exp \left[ \tilde{x}_b \frac{\xi^2 (A^{1/3} - 1)}{-\hat{t}} \frac{d}{dx_b} \right] F_{ab \rightarrow cd}(x_b) \\ & = F_{ab \rightarrow cd} \left( x_b + \tilde{x}_b C_d \frac{\xi^2 (A^{1/3} - 1)}{-\hat{t}} \right) = F_{ab \rightarrow cd} \left( x_b \left[ 1 + C_d \frac{\xi^2 (A^{1/3} - 1)}{-\hat{t} + m_d^2} \right] \right). \end{aligned} \quad (\text{B20})$$

In Eq. (B20)  $C_d = 1$  (9/4) for quarks (gluons), respectively. When  $m_d \rightarrow 0$  we recover the result of [10]. The mass here reduces the effect of power corrections and compensates for the fact that  $x_b$  already has the physical mass of parton “d” factored in.

- 
- |   |   |
|---|---|
| <p>[1] J. C. Collins, D. E. Soper, G. Sterman, Adv. Ser. Direct. High Energy Phys. <b>5</b>, 1 (1988).<br/> [2] J. F. Owens, Rev. Mod. Phys. <b>59</b>, 465 (1987).<br/> [3] M. Shimomura, [PHENIX Collaboration], nucl-ex/0510023.<br/> [4] J. C. Dunlop [STAR Collaboration], nucl-ex/0510073.<br/> [5] I. Vitev, hep-ph/0603010, Phys. Lett. B in press.<br/> [6] S. S. Adler <i>et al.</i> [PHENIX Collaboration], Phys. Rev. Lett. <b>96</b>, 032301 (2006).<br/> [7] J. Adams <i>et al.</i>, Phys. Rev. Lett. <b>94</b>, 062301 (2005).<br/> [8] I. Vitev, Phys. Lett. B <b>562</b>, 36 (2003).<br/> [9] D. Kharzeev and K. Tuchin, Nucl. Phys. A <b>735</b>, 248 (2004).<br/> [10] J. W. Qiu and I. Vitev, Phys. Lett. B <b>632</b>, 507 (2006).<br/> [11] R. C. Hwa, C. B. Yang and R. J. Fries, Phys. Rev. C <b>71</b>, 024902 (2005).</p> | <p>[12] J. W. Qiu and I. Vitev, Phys. Rev. Lett. <b>93</b>, 262301 (2004).<br/> [13] J. W. Qiu and I. Vitev, Phys. Lett. B <b>587</b>, 52 (2004).<br/> [14] S. J. Brodsky, P. Hoyer, N. Marchal, S. Peigne and F. Sannino, Phys. Rev. D <b>65</b>, 114025 (2002).<br/> [15] L. Frankfurt, V. Guzey and M. Strikman, Phys. Rev. D <b>71</b>, 054001 (2005).<br/> [16] B. Z. Kopeliovich, A. Schaefer, and, A. V. Tarasov, Phys. Rev. D <b>62</b>, 054022 (2000).<br/> [17] S. S. Adler <i>et al.</i> [PHENIX Collaboration], Phys. Rev. Lett. <b>94</b>, 082302 (2005).<br/> [18] J. Adams <i>et al.</i> [STAR Collaboration], nucl-ex/0602011.<br/> [19] J. F. Gunion and G. Bertsch, Phys. Rev. D <b>25</b>, 746 (1982).<br/> [20] M. Gyulassy, P. Levai and I. Vitev, Nucl. Phys. B <b>594</b>, 371 (2001).</p> |
|---|---|



- [21] M. Gyulassy, P. Levai and I. Vitev, Phys. Rev. Lett. **85**, 5535 (2000).
- [22] B. Z. Kopeliovich, J. Nemchik, I. K. Potashnikova, M. B. Johnson and I. Schmidt, Phys. Rev. C **72**, 054606 (2005).
- [23] I. Vitev, T. Goldman, M. Johnson and J. W. Qiu, hep-ph/0511220.
- [24] M. Cacciari, P. Nason and R. Vogt, Phys. Rev. Lett. **95**, 122001 (2005).
- [25] F. I. Olness, R. J. Scalise and W. K. Tung, Phys. Rev. D **59**, 014506 (1999).
- [26] J. Pumplin, D. R. Stump, J. Huston, H. L. Lai, P. Nadolsky and W. K. Tung, JHEP **0207**, 012 (2002).
- [27] E. Braaten, K. M. Cheung, S. Fleming and T. C. Yuan, Phys. Rev. D **51**, 4819 (1995).
- [28] D. Acosta *et al.* [CDF Collaboration], Phys. Rev. Lett. **91**, 241804 (2003).
- [29] I. Vitev, Phys. Lett. B **630**, 78 (2005).
- [30] B. A. Kniehl, G. Kramer and B. Potter, Nucl. Phys. B **582**, 514 (2000).
- [31] T. Ullrich, private communication.
- [32] J. L. Klay, private communication.
- [33] T. Alber *et al.* [NA35 Collaboration], Eur. Phys. J. C **2**, 643 (1998).
- [34] T. Itoh and H. Kato, Phys. Rev. Lett. **81**, 30 (1998).
- [35] M. Tzanov *et al.* [NuTeV Collaboration], hep-ex/0509010.
- [36] X. R. Wang [PHENIX Collaboration], hep-ex/0603051.
- [37] S. S. Adler [PHENIX Collaboration], nucl-ex/0603017.
- [38] I. Vitev, J. Phys. G **31**, S557 (2005).